ABSTRACT

ZHU, JINCHENG. Patterning Semi-transparent CNT Strain Sensors on Polymer Thin Films. (Under the direction of Dr. Philip Bradford.)

In this work, we report a novel design of a patterned CNT (carbon nanotube)/polymer strain sensor with high sensitivity. The semi-transparent CNT/PMMA (polymethyl methacrylate) thin film was fabricated by heat pressing under 135℃ and 2 tons of force while the CNT/PETG (polyethylene terephthalate glycol-modified) thin films were fabricated using a heated calendar roller. This dry-processing method avoids potential CNT degradation often seen in conventional solution-based processes. After the CNTs were embedded in the polymer film, the CNT/PMMA surface was etched into a serpentine pattern using a CO_2 laser cutter. This serpentine design is commonly used for conventional metal-foil strain gauges to increase the magnitude of sensor resistance change. The light transmission of the etched area reached 87% at 550 nm wavelength under 5% etching power and 50% speed. Quasi-static monotonic tensile tests were conducted to investigate the effects of the number of grids, width of grids, orientations of CNTs sheets, coupons and different polymer substrates on strain sensitivity. The test results of double sheet CNTs/PMMA strain sensors demonstrated that the magnitude of resistance change increased with increasing number of active grids, but on the other hand, the resistance change over initial resistance decreased since the initial resistance increased with increasing number of grids. The cross-ply sheet CNTs/PMMA strain sensors showed similar resistance-strain behavior. However, the design of cross-ply sheets CNT/PMMA allowed for decreased resistance in sensors end-loops. Use of two different substrates in this study showed that different polymer substrates could dramatically impact sensitivity of the sensors. The CNT/PETG strain sensor shows four times higher

sensitivity than PMMA based strain sensor. Some other potential applications such as temperature and pressure sensors were also investigated.

Patterning Semi-transparent CNT Strain Sensors on Polymer Thin Films

by
Jincheng Zhu

A thesis submitted to the Graduate Faculty of
North Carolina State University
in partial fulfillment of the
requirements for the degree of
Master of Science

Textile Engineering

Raleigh, North Carolina

2015

APPROVED BY:

Dr. Philip Bradford
Committee Chair

Dr. Stephen Michielsen

Dr. Chih-Hao Chang

BIOGRAPHY

Jincheng Zhu was born in Xuzhou, China on February 16, 1993. She enrolled in Kuche Secondary School which is located at Xinjiang, China. After graduating from high school, she attended Donghua University and focused on Textile Engineering. During four years in college, she had internship opportunities in Lianfa Textile Co. and Vanke real estate company, where she started to know more about industry. Then she decided to study further abroad after graduation from college. She continued to pursue a master degree major in Textile Engineering at the College of Textiles in North Carolina State University in 2013. At the end of her second semester, she joined Dr. Bradford's research group and became a graduate researcher. She focused on the study CNT/polymer thin film as high sensitive strain sensors. During this research period, she gained lots of knowledge about engineering and science and got lots of hands-on experience.

ACKNOWLEDGMENTS

First of all, I would love to sincerely thank my advisor Dr. Philip Bradford for guiding me, and always being patient with me throughout the whole research and thesis-writing process. Thanks to his dedication, I gained lots of knowledge and build up a thoughtful mind as a good researcher.

And I also want to appreciate every group member in this research group. I could not finish my work without you guys help. Ang, Brian, James, Karim, Kelly, Kevin, Ozkan, Shaghayegh, Spencer, thanks for everybody's time and work. I would like to thank Ang and Karim who are always willing to spend their time on helping me with my tensile test. Thank to Spencer for always helping me out in sample-making process. I also appreciate Ozkan help me perform CNT growth. And a special thank you to Kelly and James who are always willing to answer any question along my whole research process. I also would like to appreciate lab manager Birgit and Judy for training me using UV-Vis spectroscopy and SEM. And a special thanks to Xiaomeng Fang in Dr. Ghost's research group who is always willing to measure sheet resistance for me.

In the end, I would love to thank all my family members, my mom, dad, sister and beloved husband Chu. Thank you Chu for always support me and always with me been through all the hard time I've experienced these two years.

TABLE OF CONTENTS

LIST OF TABLES

LIST OF FIGURES

1 Introduction

Determining the stress and strain distribution in structural materials is of critical importance. It is the motivation for the development of various technologies for detecting stress. However, there is no direct way to measure stress. Therefore, the strain measurement is an alternative way to determine stress by mathematical formula. Nowadays, the most commonly used strain sensor is metal-foil strain gauge. It has been well-developed and used for decades, yet it still has lots of limitations in application such as opacity, rigidity and low gauge factor. Therefore, the main goal of this research is trying to find another way to fabricate new strain gauges by using CNT/polymer thin film to solve those issues while at the same time producing sensors which have the added functionality of being semi-transparent.

Transparent electrical devices such as touch screens, displays and solar cells have been well-developed and became prevalent in recent years. Because of its electrical conductivity and optical transparency, indium tin oxide (ITO) has been the most common material for the application of transparent electrical devices. However, due to high cost, less flexibility, and low supply, many researchers have attempted to engineer alternative materials to take place ITO. Carbon nanotubes (CNT) and graphene are among those popular alternatives. In our research, we will mainly focus on CNTs.

The excellent electromechanical properties of CNTs make them a good candidate for strain sensing applications. One promising application of CNTs is in CNT/ polymer thin film strain

sensors. Methods for fabricating CNT/polymer nanocomposites have been reported before, and they usually are synthesized by mixing random oriented CNTs with a polymer solution. Many studies show fabrication of CNT/Polymer nanocomposites through solution mixing or film casting, melt compounding, and in situ polymerization (Thomas & Zaikov, 2008a). The problem of those methods is that when ultrasonication is used to disperse CNTs, it may also cause damage to CNTs. Also it is hard to predict the performance of this kind of material because of the random orientations of dispersed CNTs in polymer. With the production of high quality CNT arrays (also called CNT forest), continuous CNT sheet production has become available. Compared to solution-based method, dry-processed CNT sheets from drawable CNT arrays could avoid some complicated processing such as sonication, purification and centrifugation which could dramatically simplify the fabrication process. Thus, in our study, we will fabricate sensors by drawing the CNT sheet across a thin polymer film and then use heat to embed the CNTs in the surface of the polymer. This method could save lots of time and also protect CNTs from damage in processing. The aligned CNT sheet is also anisotropic which could help to fully take advantage of superior properties of CNTs.

Another innovative method has been used in this study is etching serpentine patterns on CNT/ polymer thin films. In this research, we will discuss a new technique which involves laser etching for patterning CNT/polymer thin films. This serpentine pattern is commonly used in conventional metal-foil strain gauges. The theory behind this pattern is also same as metal foil strain gauge. The stress applies in the direction of parallel active grids will make

the strain gauge thinner and longer, with multiple grids providing a much higher resistance change than just one single conductive line. At the same time, the fabricated sensors will be semi-transparent which may useful in strain sensing in transparent structural materials or other optoelectronic applications.

This work will be the first known to demonstrate sensors where aligned CNTs are embedded on the surface of polymer films and then etched into patterns to increase the sensitivity of the strain sensing devices.

2 Literature Review

2.1 Carbon nanotubes

2.1.1 Carbon nanotube background

Since Iijima brought carbon nanotubes to the attention of the scientific community in 1991, they have drawn the attention in many researchers. Due to their high mechanical strength, elastic modulus, electrical conductivity and thermal conductivity, CNTs have been highly studied in recent years. Statistically, the trend of publications and patents about CNTs is shown in figure 1. From 1990 to 2006, the number of articles on the subject of CNTs increased significantly.

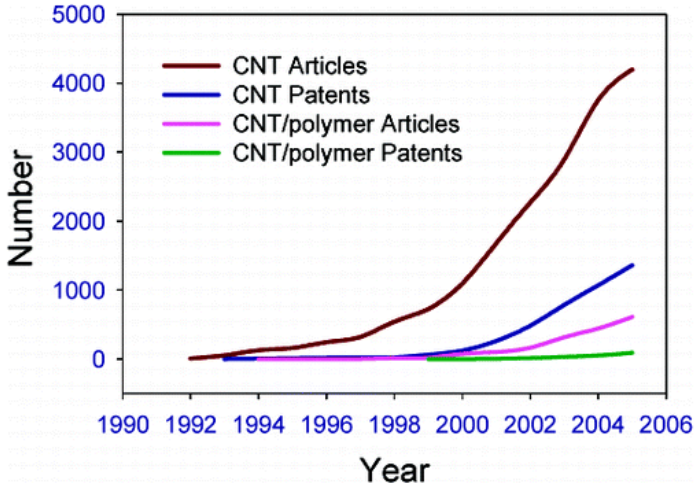

Figure 1. Number of published articles and patents on CNT and CNT/polymer (Moniruzzaman & Winey, 2006).

A CNT is a long seamless cylindrical structure with sp^2-bonded carbon graphite sheet. There are three kinds of CNTs which are categorized by the number of nanotubes walls: Single-wall carbon nanotube (SWCNT), double-wall carbon nanotube (DWCNT), and multi-wall carbon nanotube (MWCNT). SWCNT is considered a seamless graphene sheet rolled up, while DWCNT and MWCNT rolled up by two and more layers graphene sheets respectively. The morphology of SWCNT and MWCNT can be observed under high resolution transmission electron microscope (TEM) (Figure 2). For SWCNTs, they have smaller diameters compare to MWCNT. Statistically, the mean diameter of SWCNT is range from 1.0 to 1.5 nm. The difference between inner and outer diameter of MWCNTs falls between 5 and 100nm (Schulz, Shanov, & Yin, 2013).

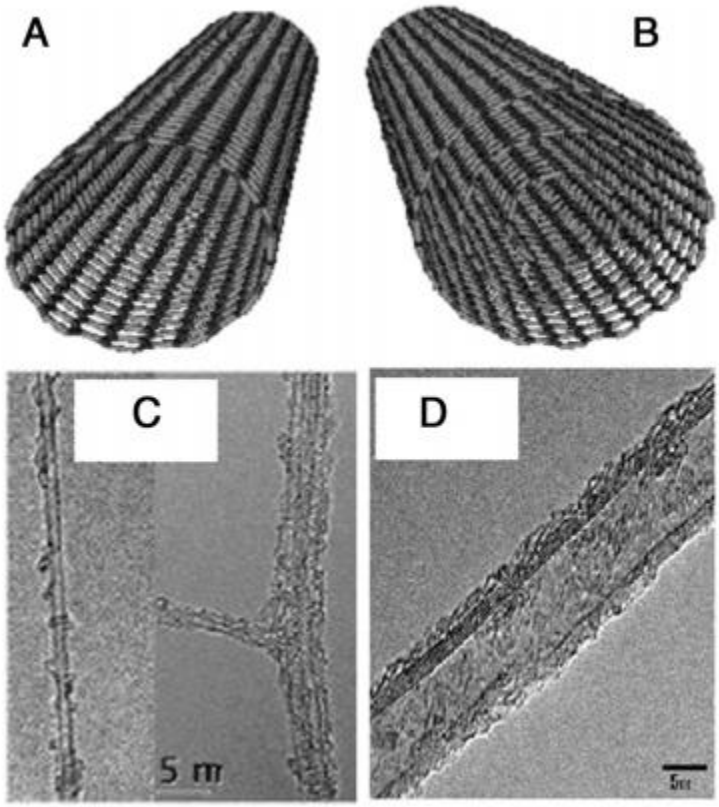

Figure 2. Schematic structure of (a) SWCNT (b) MWCNT; High-resolution TEM images of (c) SWCNT (d) MWCNT (Eatemadi et al., 2014).

CNTs have outstanding mechanical properties, electrical properties, thermal properties and electromechanical properties compared to many conventional materials. This review will shed light on these fascinating properties of CNTs. Many researchers show a large interest in mechanical properties of nanotubes due to the strength of C-C bonds. Because CNTs are made up of seamless hollow graphene cylinders, it is expected to see CNTs possess extreme mechanical properties. Theoretically, the elastic modulus of SWCNTs is around 2.8 to 3.6 TPa and MWCNT is 1.7 to 2.4 TPa. In reality, the experimental elastic modulus value of

SWCNT has been reported to be approximately 1470 GPa and MWCNT is 950 GPa, which is five times higher than steel (Choudhary, Singh, & Mathur, 2013). The tensile strength of CNTs usually falls in the range from 11 to 63 GPa (Arash, Wang, & Varadan, 2014).

In terms of their electrical properties, CNTs can be considered either metallic or semiconducting. SWCNT can exhibit either metallic or semiconducting character depending on the geometry of nanotube walls and band gaps. For MWCNT, the electrical property could alternative between metallic and semiconducting randomly but because of the multiple walls, are considered metallic (Bandaru, 2007). Especially for metallic CNTs, the electric current density could be as high as 4×10^9 A/cm^2, almost 1,000 times higher than copper. The axial electrical conductivity will be deteriorated significantly by defects and as the number of walls increases (Arash et al., 2014).

In Che et al.'s work, they found that thermal conductivity of CNTs is higher than diamond crystal and graphite sheet. The anisotropic thermal conductivity of graphite also influences the CNT thermal behavior (Che, Çagin, & Goddard, 2000). Han et al. reported that thermal conductivity of CNTs at 25℃ ranges from 2000 to 6000 W/m K whereas graphite is from 100-400 W/m K and diamond is 2000 W/m K at the same 25℃ temperature (Han & Fina, 2011).

In the literature, theory has explained that the electromechanical properties of SWCNTs depend on nanotube chirality. The electrical properties of armchair metallic M-SWNT (m=n) should be the least sensitive to tensile strain due to their high symmetry. Other types of SWCNTs, including quasi-metallic and semiconducting nanotubes show higher sensitivity and exhibit band-gap change under tensile strain (Cao, Wang, & Dai, 2003). The electrical properties of MWCNTs, on the other hand, are not subject to chirality-related restrictions (Vemuru, Wahi, Nagarajaiah, & Ajayan, 2009).

The mechanical deformation can alter band gap structure of CNTs, which cause the effect of electronic property change. Minot et al. reported that the band structure of CNTs can be altered by mechanical strain. The band gap in metallic nanotubes can open and in semiconducting nanotubes can be modified by mechanical strain (Minot et al., 2003). In Heyd et al. work, they have shown that CNTs can modify the band gap significantly and induce a semiconductor-metal transition with applied uniaxial stress (Heyd, Charlier, & McRae, 1997). The periodic boundary condition caused by rolling a seamless graphene sheet into a nanotube should be taken into considered in the electronic structure of CNTs, which results in the quantization of the tube electron wave functions. The alter in the conic section is attributed to the change of CNTs bond length by shifting the quantization period during strain applying, which cause the decrease or increase the band gap (Obitayo & Liu, 2012).

2.1.2 Carbon nanotube structure

The way the graphene layer is rolled into the tube can be represented by a pair of indices (n,m). The equation of graphene 2D lattice vector is $C_h = n \cdot a_1 + m \cdot a_2$, where a_1 and a_2 are unit vectors. There are three kinds of orientations of atoms around the cylinder: arm chair i.e. up-down-down-up (Figure 3(b)), zigzag i.e. up-down-up-down (Figure 3(c)) and chiral which combines arm chair and zigzag features together (Figure 3 (d)). The SWCNTs are called arm-chair if $n = m$. They are called zig-zag if $m = 0$, and the rest are called chiral where $n > m > 0$ (Rao, Voggu, & Govindaraj, 2009). Based on the structure, the CNT can have either metal or semiconducting properties. If $n = m$, the armchair CNT exhibits metallic behavior, zigzag CNTs (n,0) can be either metallic if $n = 3q$ (q is an integer) or insulating, and chiral structure SWCNT could exhibit metallic if $n - m = 3 \cdot i$ (i is an integer) (Kanoun et al., 2014a). Based on statistical results, a natural mix of CNTs should contain $\frac{1}{3}$ of metallic and $\frac{2}{3}$ of semiconducting (Majumder, Kaushik, & Manhas, 2011). But in reality, the geometric structures of CNTs are more complicated due to presence of defects. Thus the electrical properties are more complex compared with perfect CNTs.

MWCNTs usually consist of multiple layers of graphene with different structures. The spacing between adjacent layers is about 0.34 nm. The aspect ratio of MWCNTs varies with diameter but usually the length is 100 times longer than the diameter, and even much higher in some special cases. The conductivity of MWCNTs is complicated but it always exhibits metallic behavior. The way how electrons go through nanotube for MWCNTs is similar to

SWCNTs because electrons are restricted by outermost tubes. The three characteristic properties of MWCNTs that have drawn the most attention are: electrical conductivity near that of copper, mechanical strength is 15 to 20 times stronger than steel and at the same time five times less dense, and thermal conductivity similar to diamond (Cefic, 2013).

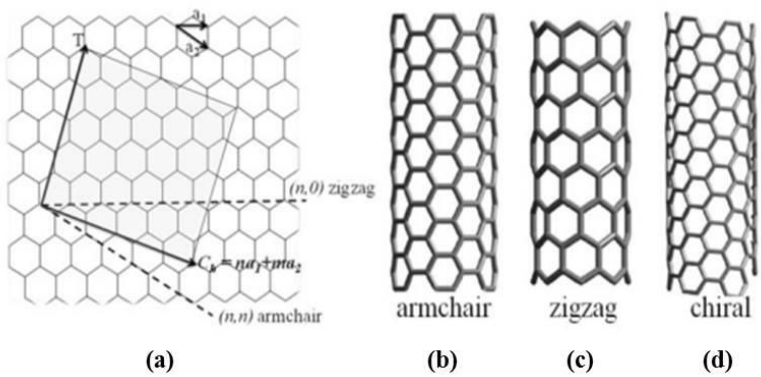

Figure 3. Different constructions of CNTs (Kanoun et al., 2014b).

2.1.3 Carbon nanotube synthesis

Since the discovery of CNTs, the methods of producing them in large scale, with low impurities and lower cost has been widely discussed and attempted. So far, the most common techniques to synthesize CNTs are arc discharge, laser ablation, and chemical vapor deposition (CVD) (Rafique & Iqbal, 2011a).

Arc discharge is one of the oldest methods to produce CNTs. Initially this method was used to manufacture C60 fullerenes. This manufacturing setup has inert gas flow in the reaction vessel which is controlled at low pressure. The arc is generated by applying direct current which causes potential difference between two electrodes which are made of graphite. CNTs are created by plasma discharge between the two electrodes (Figure 4 (a)) (Choudhary & Gupta, 2001). However this technique will cause impurities such as carbon soot, amorphous carbon and residual metal catalyst which may contaminate final CNTs product. Therefore the mixed components need further purification. This method is mainly for SWCNTs production. There are some limitations for producing SWCNTs in term of quantities and typically they are very expensive even at the gram scale.

Laser ablation, a pulsed laser deposition process, can grow high-quality and high-purity (up to about 90% pure) SWCNT. In this process, a laser beam is shot at a graphite target containing metal catalyst (Ni or Co) in high-temperature furnace (1200 ℃) in an inert atmosphere (Figure 4 (b)) (Prasek et al., 2011). The final CNT product will be deposited on the cooler reactor surface. In this technique, the main impurities are amorphous carbon and residual catalysts.

Both arc discharge and laser ablation are ideal methods to produce high-quality CNTs. However, the inherent design of these two systems causes limitations in the production rate of these high quality CNTs (Burdick et al., 2011). In addition, due to vaporization involved

in these two CNT manufacturing processes, the final products are in highly tangled forms and also mixed with different impurities. Thus, the CNTs produced are hard to purify (M.N.Avadhanulu, 2007).

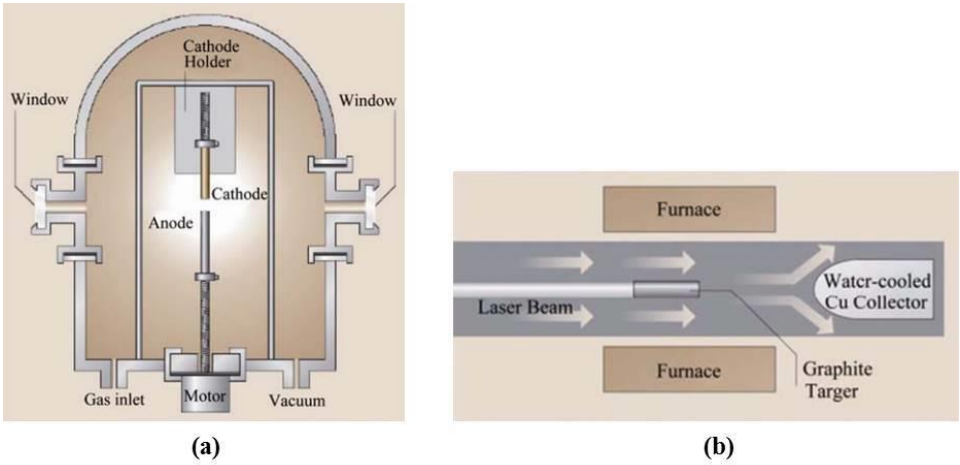

Figure 4. CNT production models (a) Arc discharge (b) Laser ablation (Rafique & Iqbal, 2011b).

Chemical vapor deposition (CVD) is a chemical process for producing thin solid films on a substrate surface by thermal deposition of reactive gaseous compounds. During the CVD process, the volatile precursors will react or decompose on the substrate surface (Choy, 2003). CVD is method used in scale-up process for CNT growth. Compared to the two CNT-synthesis techniques mentioned before, CVD has the advantages of simplicity and lower cost. The CVD manufacturing process of CNTs is conducted at relatively low temperature and often ambient pressures (Kumar & Ando, 2010). CVD usually produces longer CNTs

compared to arc charge and laser ablation but with more defects (Nessim, 2010). Many companies now produce ton quantities of CNTs using this method.

Catalyst materials for CVD processing are usually transition metals such as Ni, Co, Fe, Al or Mo (Moshkalyov, Moreau, Guttiérrez, Cotta, & Swart, 2004). There is also a wide variety of carbon precursors that can be used in CVD method such as methane, acetylene or ethane. The reactor typically constitutes a quartz tube placed in a tube furnace (Figure 5). The reaction temperature typically ranges from 500 to1000 ℃ to decompose the precursor gases and to heat the sample (Kumar & Ando, 2010).

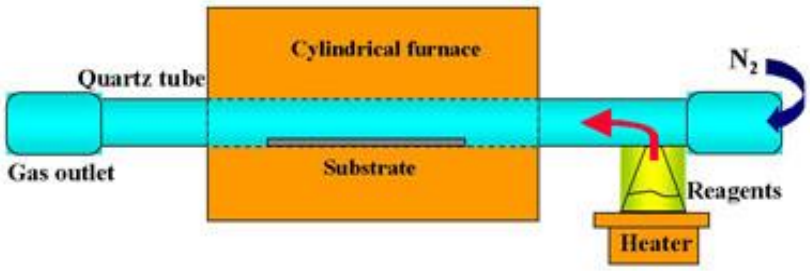

Figure 5. CNTs Growth by chemical vapor deposition (CVD).

Most CNTs produced using CVD are relatively short and in powder form, which decreases length-dependent properties such as electrical and thermal conductivities, and mechanical strength and modulus (Lepró, Lima, & Baughman, 2010). Under the right processing conditions, CNT arrays can be grown on substrates and these arrays if produced with high

enough quality can produce drawable CNT arrays (Figure 6). It has been proven that long CNTs will improve strength and electrical properties (Times & Central, 2009). The ability to synthesize drawable CNT arrays directly offers the potential for these long, aligned CNTs to be used in novel applications and materials that can benefit from the unique CNT structure (Huynh & Hawkins, 2010).

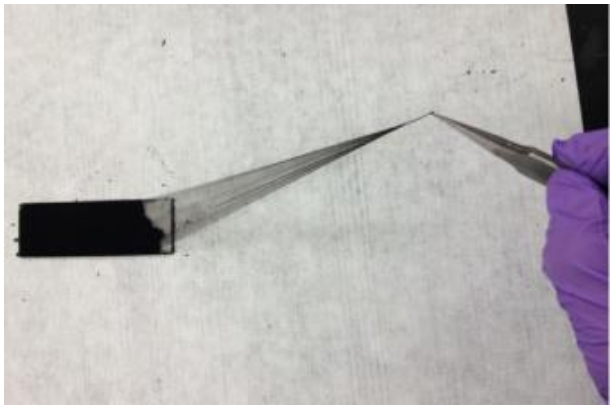

Figure 6. Drawable CNT array (Yildiz & Bradford, 2013).

Kuznetsov et al. came up with a structural model to explain the mechanism of dry-drawing sheets from drawable CNT arrays. The key element of this model is a network of the array of big CNT bundles surrounded by interconnecting small bundles or individual CNTs (Figure 7 left). The idea is that two big CNT bundles are connected by a single connection like shown in figure 7. Under the horizontal external force, the vertically aligned big CNT bundle will reorient into horizontal direction. The connection between the two big bundles is detached

from the left bundle during the drawing process and is adhered to the right one due to the Van der Waals force. This process is called “unzipping”. As the drawing process continues, the connections concentrate at either CNT array top or bottom alternatively, which is forming the final sheet or yarn (Kuznetsov, Fonseca, Baughman, & Zakhidov, 2011).

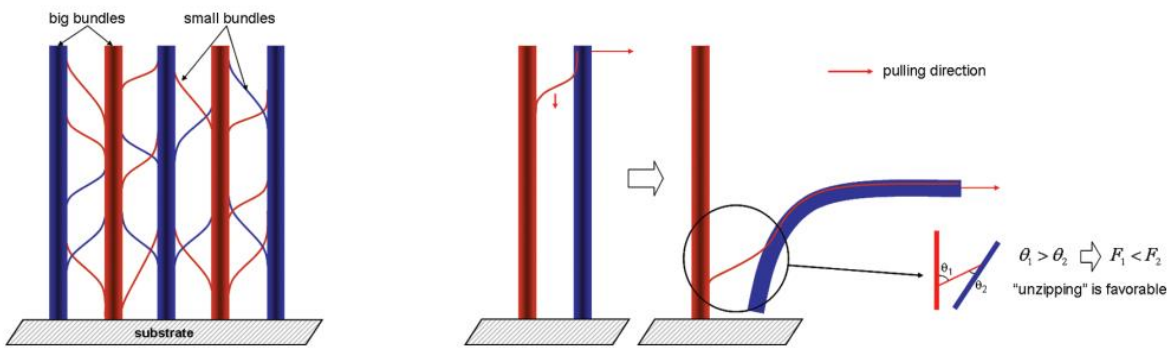

Figure 7. Schematic picture of vertically aligned big CNT bundles and interconnecting small bundles or individual CNTs (Left). The unzipping-zipping process with the external force results in the interconnecting small bundles or individual CNTs concentrate at array ends between adjacent big CNTs bundles (Right) (Kuznetsov et al., 2011).

2.2 CNT/Polymer film fabrication and application

2.2.1 Strain gauge background introduction

The demand for determining stress and strain distributions inside of structural parts has stimulated the development of various technologies for measuring stress/strain. Strain could be converted to stress by equation:

$$\sigma=\varepsilon\times E$$

σ: stress; ε: strain; E: modulus

There are several ways to measure strain, but the most widely used one is the strain gauge. Technically, any device that can sense structural deformation should be considered a strain gauge. Among those devices, the most commonly used are the electromechanical type metal-foil strain gauge. Commercial metal-foil strain gauges usually consist of a strain-sensing alloy, backing material and lead wires. The crucial component for sensing deformation is the strain-sensing alloy. Strain-sensing alloy is a very fine and thin wire looped into serpentine pattern in strain gauge. A variety of strain gauge alloys are supplied to the market such as Constantan, Isoelastic and Karma. Constantan (45% Ni, 55% Cu) is the oldest but still the most commonly used strain-sensing alloy due to the best combination of properties. For example, it has relatively high strain sensitivity and high resistivity to achieve a high resistance value even in small gage. Due to its great thermal stability, temperature change doesn't have a significant influence when it is used on structural materials. Also, Constantan shows excellent fatigue life and relatively high strain range (up to 8%). Isoelastic (36% Ni, 55.5% Fe, 8% Cr, 0.5% Mo) and Karma (74% Ni, 20% Cr, 3% Al, 3% Fe) are usually applied in other special cases. For instance, because of good sensitivity and fatigue strength, the isoelastic alloy is used in dynamic and fatigue applications. Karma alloy represents good stability and self-temperature-compensation so that it could be used for precise static

measuring over a long period time and also a larger temperature range (Khan & Wang, 2001).

The backing material works as both insulator and carrier for the strain-sensing alloy. It also provides a practical way to bond the strain gauge on specimen surface easily. Two basic backing materials types are polyimide and glassfiber reinforced epoxy-phenolic. Polyimide is a desired material for most static and dynamic stress analysis with large temperature range from -195° to +175°C and large strain range up to 20%. Glassfiber reinforced epoxy-phenolic backing material has outstanding performance over large temperature range from -269° to + 290°C for static and dynamic measurements.

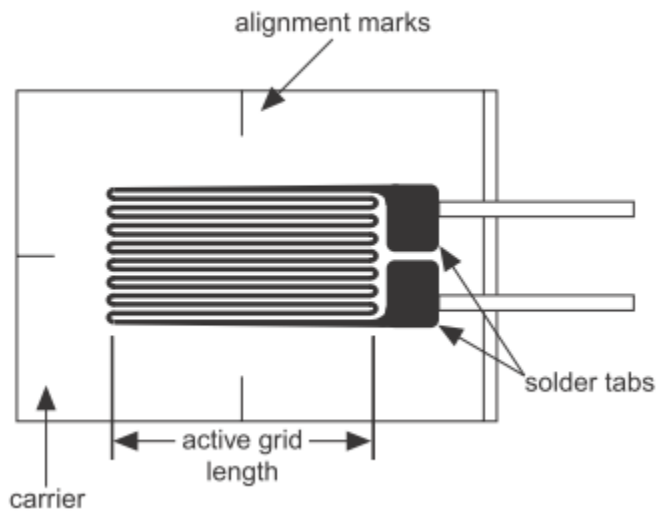

Figure 8. Schematic of typical metal-foil strain gauge.

The operation principle of metal-foil strain gauge is that when the conductor is subjected to an applied stress in axial direction, the length of this direction will increase and also, the cross-sectional area will decrease due to the Poisson ratio. In addition, the specific resistivity of conductor may change as well. Therefore, these three factors will cause overall resistance increases according to:

$$R=\rho\frac{L}{A}$$

ρ: specific resistivity; L: length; A: cross-sectional area

The sensitivity of strain gauges is expressed by the gauge factor. Gauge factor is the normalized change in resistance versus strain as the following equation:

$$\text{Gauge factor (GF)} = \frac{\Delta R}{R_0}\frac{1}{\varepsilon}$$

$R_{0:}$ initial resistance, ε: strain

The procedure for bonding a metal-foil strain gauge on structure's surface is crucial in order to achieve precise strain measurement. A poor bonding quality will not effectively transfer strain. The details on properly preparing the structure's surface to mount the strain gauge on the surface will be introduced in chapter 3.2.6.

Even though metal-foil strain gauges have been around for a century and fill more than 80% of the strain-sensing market in the United States, there are still many problems with commercial metal-foil strain gauges. Positioning strain gauges on specimen surfaces can be

tricky. If one wants to investigate the behavior of an area of high stress concentration such as crack or fillet radius, this can be challenging. Most commercial metal-foil strain gauges are opaque, meaning that the high stress concentration area could be missed when mounting the strain gauge on specimen surface. Also, some conformal strain sensors used on area of the human body need to be invisible during daily activities (Elastomers et al., 2015). Therefore, there is a demand for semi-transparent or transparent strain gauges. In terms of strain sensitivity, usually the resistance value of commercial metal-foil strain gauge is 120Ω or 350Ω with gauge factor is 2.0 or 2.1. Also, conventional metal-foil strain gauges are considered brittle and rigid, however, strain gauges are sometimes needed to cover movable or arbitrarily shaped objects in some specific applications such as attach on human skin and embedded into garments.

Since there are some issues with conventional metal-foil strain sensor, other alternatives for strain sensing materials have been studied. CNTs are an ideal material that could be used in the electrical-resistance strain sensing field since they exhibit piezoresistivity, which means there is a change in resistance when mechanical strain is applied (Yong, Wanlu, Kejun, & Chenguo, 2003). In CNTs, only the lowest sub-band plays a role of changing the band gap so that the resistance will change. Because the second sub-band of conduction band is about 1 eV higher than the lowest sub-band, it is too high to have large carrier population. The overall number of carriers will change if the band gap changes, which causes the overall resistance change (O’Connell, 2006).

CNT are strong, elastic and can be bent to small radii without breaking (Kang, Schulz, Kim, Shanov, & Shi, 2006). Yamada et al. fabricated vertically aligned SWCNT thin film strain sensors on a dog-bone shape polydimethylsiloxane substrate which could be embedded into clothing or attached on skin. The vertical aligned SWCNT thin films develop gaps which influences the electrical properties of the film and worked as strain sensor, with a maximum change in resistance up to 280% (Yamada et al., 2011). Chang et al. reported a simple way to fabricate flexible SWCNT strain sensor by transferring aligned SWCNT synthesized by CVD from a silicon substrate to a flexible substrate. This strain sensor showed remarkable flexibility (N.-K. Chang, Su, & Chang, 2008). Cai et al. fabricated super-stretchable, transparent CNT-based strain sensors for bio-interactive application (Figure 9). The CNT-based strain sensors detected strains in the range of 1% to 300% and also the transmittance of as-produced strain sensors was as high as 90% at 550 nm wavelength (Cai et al., 2013).

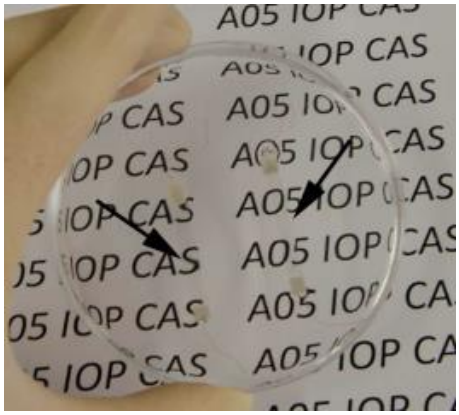

Figure 9. Optical picture of two strain gauges in a petri dish(Cai et al., 2013).

Many research studies to study CNT piezoresistivity properties show that CNTs are an excellent candidate for strain sensing application. In the following section, fabrication methods, CNT strain sensor properties and applications will be discussed.

2.2.2 Fabrication methods for embedding CNTs on planar surface

There are variety ways to embed CNTs into polymers. Three processing techniques were reported in literature for fabricating CNT/Polymer nanocomposites are solution mixing or film casting, melt compounding, and in situ polymerization (Thomas & Zaikov, 2008b). These techniques have to mix carbon nanotubes and polymer together using different methods, as summarized in figure 10. The high shear forces usually involved in this process degrade CNT and polymers properties. Also, the process is complicated and with lots of steps involved. Therefore, in this work, we only focus on fabrication methods where CNTs are embedded on planar polymer surfaces.

Suspension-based methods usually are used to deposit CNTs networks on flat surfaces. Common methods can be categorized into electrophoretic deposition, spin coating, spray coating, dip coating, vacuum filtration (Figure 11) (Saha, Jiang, & Martí, 2014).

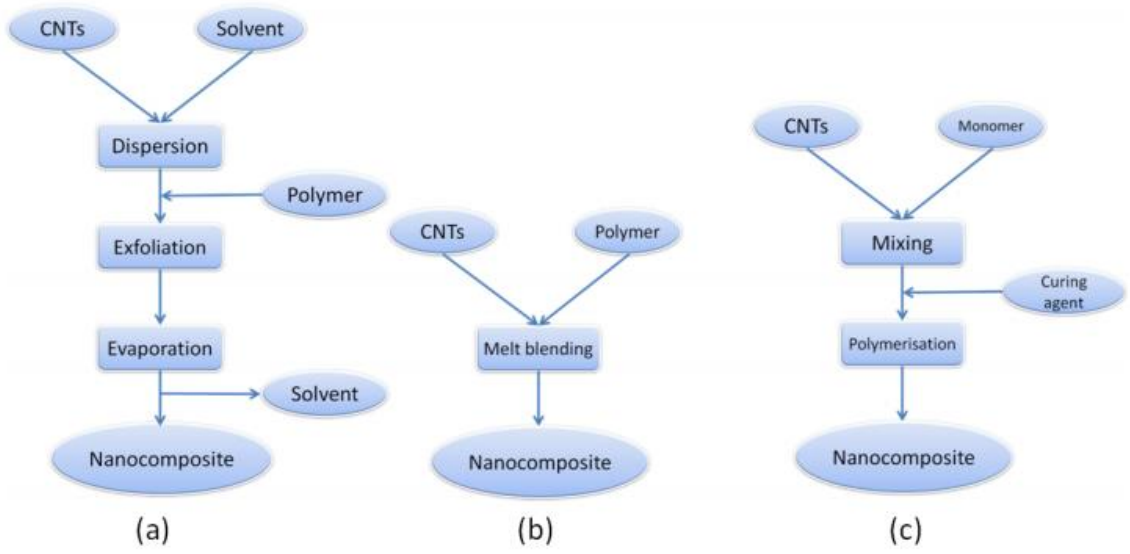

Figure 10. Different carbon nanotube/ polymer nanocomposites manufacturing process: (a). Solution mixing or film casting (b) melt compounding (c) in situ polymerization (Beyou, Akbar, Chaumont, & Cassagnau, 2013).

In the electrophoretic deposition (EPD) process, there are two essential steps involved in the EPD process. In the first step, charged particles dispersed in a solvent will migrate towards the desired electrode under the applied DC electric field. Then the particles adhere and form a deposition on the electrode surface (Sarkar & Hah, 2012). Chang et al. research showed that they actually synthesized transparent SWCNTs networks on planar PET substrates for strain sensing by spray coating. First, they dispersed and sonicated SWCNTs in solution by controlled SWCNT volume. Then they sprayed CNT film on adhesive-coated PET substrate and a pair of Pt electrodes were placed on the ends, as shown in Figure 12 (W. Chang, Song, Kim, & Kim, n.d.). Spin coating consists of dropping a CNTs solution on a high speed rotating substrate (Cueto, Ma, Chinesta, & Mackley, 2008). The centrifugal acceleration

spreads the solution and the thickness can be controlled by changing the solution viscosity and spinning speed. Mirri et al synthesized transparent conductive CNTs films by dip coating. They dissolved SWCNT and DWCNT in chlorosulfonic acid (CSA) and then withdrew a glass slide from the solution with the CNT film forming on the surface (Mirri et al., 2012). Saotome et al. fabricated transparent conducting CNT films by vacuum filtration. The CNTs were dispersed in oleum by sonication for certain time and temperature. The monodispersed solution was then vacuum-filtered to obtain a thin film (Saotome, Kim, Wang, Lashmore, & Hahn, 2011).

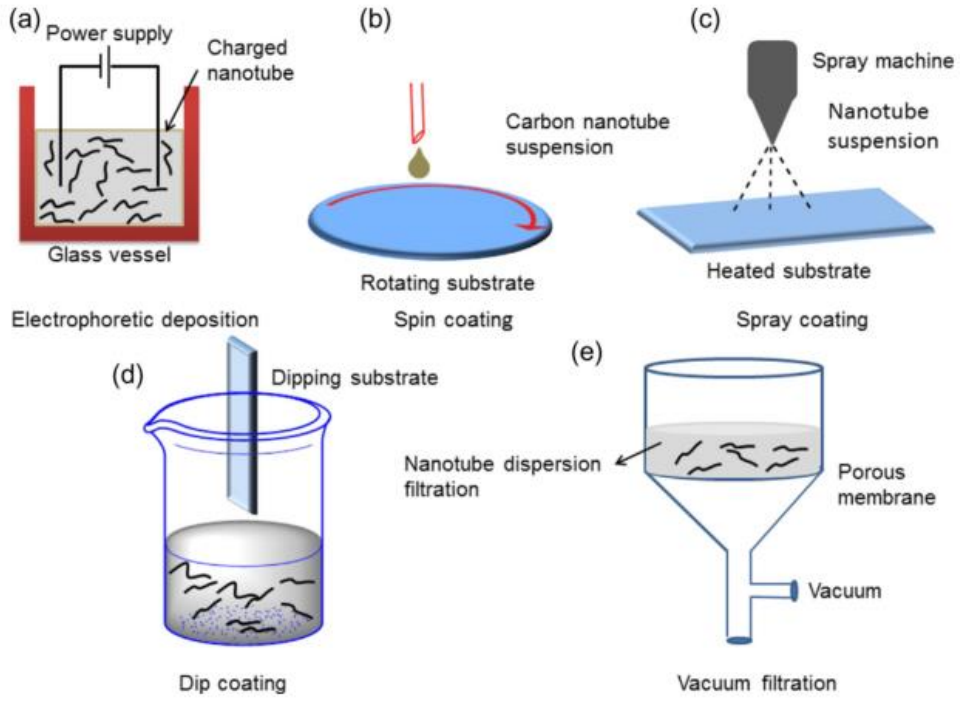

Figure 11. Embedding CNT on planar surface fabrication methods. (a)electrophoretic deposition (b)spin coating (c)spray coating (d)dip coating (e)vacuum filtration (Saha et al., 2014).

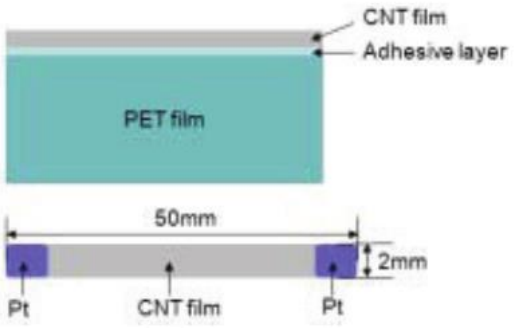

Figure 12. Spray coating CNTs network on PET substrate with a pair of Pt electrode (W. Chang et al., n.d.).

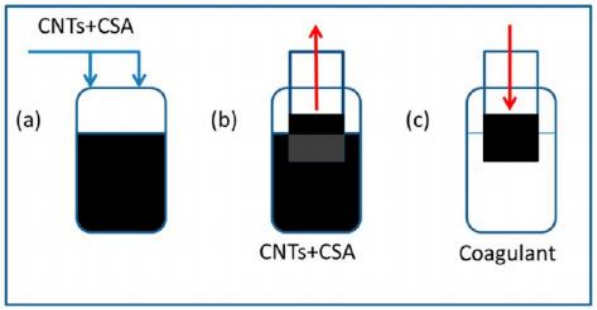

Figure 13. Dip-coating process (Mirri et al., 2012).

The method used in this study is to apply an aligned CNT sheet on a planar polymer surface. While stretching CNTs from drawable CNTs array, CNTs tend to attach end to end because of strong Van der Waals force which helps forming uniform aligned CNT sheet (Figure 14). In Barbour et al.'s work, they introduced a novel method to fabricate aligned CNT sheet onto

PETG thin films at high temperatures and pressure using a calendar system. The transparency of the CNT/PETG thin film reached as high as 70% (Barbour, 2014).

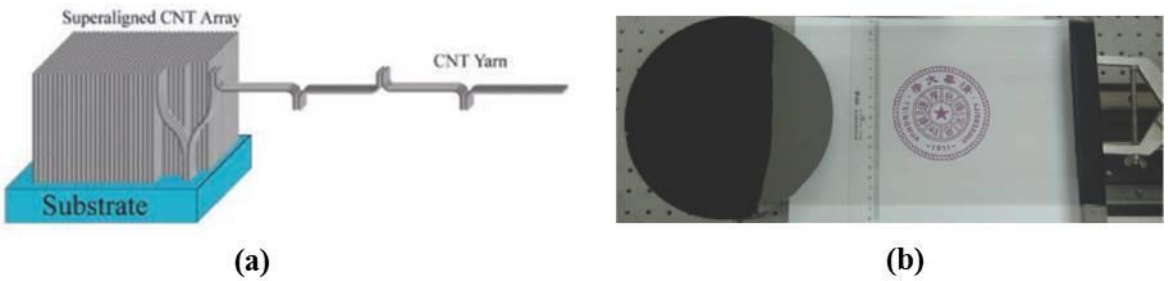

Figure 14. (a) Schematic elucidation of CNTs attach end to end when stretching (b) Uniform aligned CNT sheet (Jiang et al., 2011).

A new finding about conductivity and piezoresistance of MWCNT/ thermoplastic polymer films were reported by Oliva et al. MWCNT/ polymer films with randomly distributed CNTs were aligned using an electric field. The study showed that an increase in alignment of the CNTs in the polymer will increase the electrical conductivity and strain sensing ability (Oliva-Avilés, Avilés, & Sosa, 2011). However, the highest strain gauge reported in this study is about 2.78 which just a little bit higher than traditional commercial metal foil strain gauge.

Other ways to improve CNT alignment in polymer matrices have been reported in the literature. In Jin et al.'s work, they improved the alignment of dispersed CNTs in polymer by applying mechanical stretching (Jin, Bower, & Zhou, 1998).

2.2.3 CNT/Polymer strain sensing applications

Conventional strain sensors have limitations in many applications because of high stiffness, opaque and low strain at plastic deformation. More and more researchers have shown an interest in fabricating flexible, transparent CNT/Polymer thin film strain sensors. So far, the piezoresistivity of CNT/polymer strain sensors could be categorized in three types: loss contact points between CNTs, tunneling resistance change between CNTs (Figure 15) and intrinsic piezoresistive nature of CNTs under deformation (Hu et al., 2008).

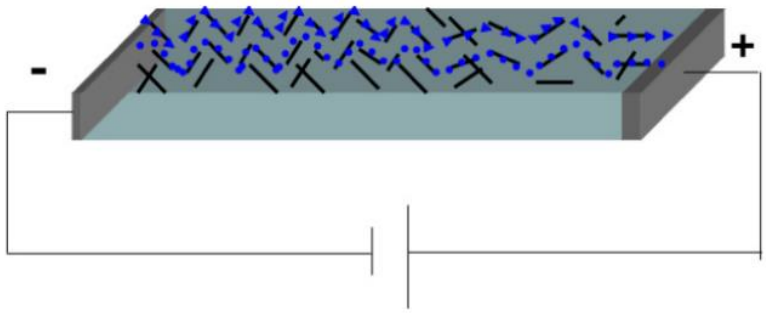

Figure 15. Electron tunneling pathway through CNT/Polymer nanocomposite (Gau, Kuo, & Ko, 2009).

In Pang et al. work, they fabricated a highly flexible, multiplexed and real-time sensors that could be used as skin-attachable or skin-like electronic sensors (Pang et al., 2012). A highly deformable CNT/elastic polyurethane nanocomposite strain sensor was made by Slobodian and his coworkers. Testing showed that this kind of material could be stretched as high as 400% while the resistance increased more than 270 times (Slobodian, 2012). Xu et al. developed a MWCNT/polydimethylsiloxane (PDMS) composite patterned strain sensor which had gauge factors ranging from 13 to 120 (Xu & Allen, 2013). Jung et al. reported a novel way to fabricate transparent MWCNT/PDMS strain sensors. They actually drew CNTs sheet from CNT forest and embedded into PDMS (figure 16 (b)) instead of disperse CNTs in solution. The sensitivity of this kind strain sensor could be as high as 30.1 (Jung, Lee, Overzetand, & Lee, 2012). Studies also show that high strain sensitivity could be reached at a critical CNT filler content which called percolation threshold. The conductivity of CNT/ polymer nanocomposite could increase significantly at percolation threshold due to the conducting path forms which cause sensitivity is higher too. Percolation threshold values strongly depend on CNT type, CNT aspect ratio, polymer type and manufacturing process (Kanoun et al., 2014a)

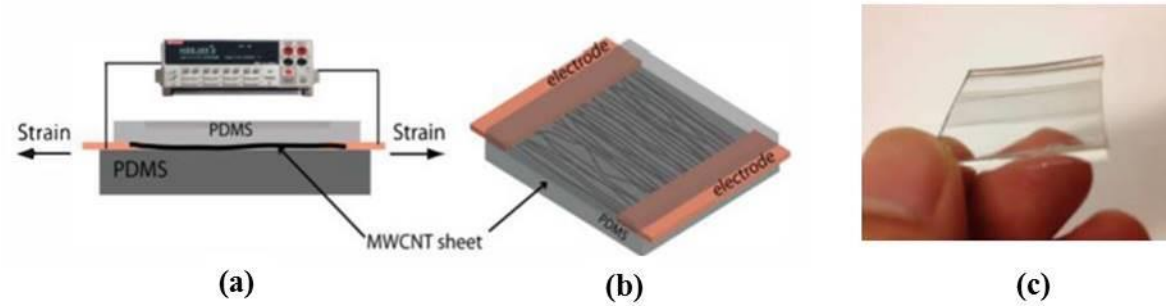

Figure 16. (a) Electromechanical experiment set-up; (b) CNTs sheet embed into PDMS; (c) Transparent MWCNT/PDMS strain sensor (Xu & Allen, 2013).

2.2.4 New trend: patterned CNT/polymer thin film

Since CNT/ polymer thin films show lots of promising applications in many fields, more and more researchers are interested in improve their performance by adding different patterns. One important technique used to pattern CNT/polymer films is etching. However, selective CNT etching processes are very complicated and researchers are developing new methods to simplify this process.

Kim et al. reported that they fabricated patterned CNTs on both recessed and flat polydimethylsiloxane (PDMS) surfaces, which could be used in sensors or electronics, by a simple and low-cost photolithography technique. As shown in figure 17, this sensor is highly flexible and transparent, and also show high gauge factor ranging from 2 to 6 (Kim & Yun, 2013).

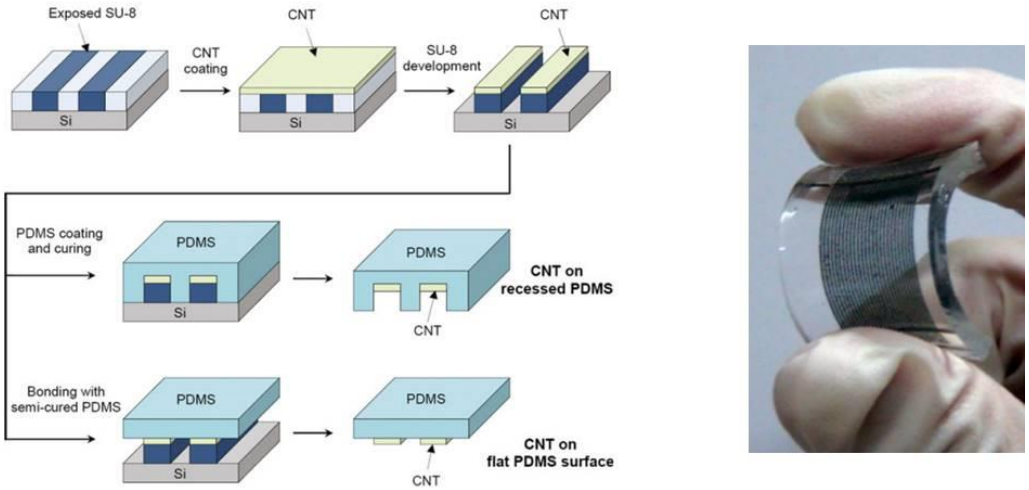

Figure 17. Patterning of carbon nanotube films on PDMS (Kim & Yun, 2013).

Lee et al. proposed a way to fabricate SWCNT film strain gauge for sensing application. The procedure is shown in the left image of figure 18. Polyimide was spin-coated on substrate and then Cr film evaporated on it. Finally SWCNT film was spray-coated over PI and Cr following with home-made O_2 plasma etching. They've tried different numbers of grids such as 4, 6, and 8. The result shows (figure 18 right) that over a range from 0 to 400 micro strain, 8 grids had the highest gauge factor of 16.1 which is approximately eight times higher than conventional metal foil strain gauges (Lee, Hong, Lee, Park, & Min, 2011).

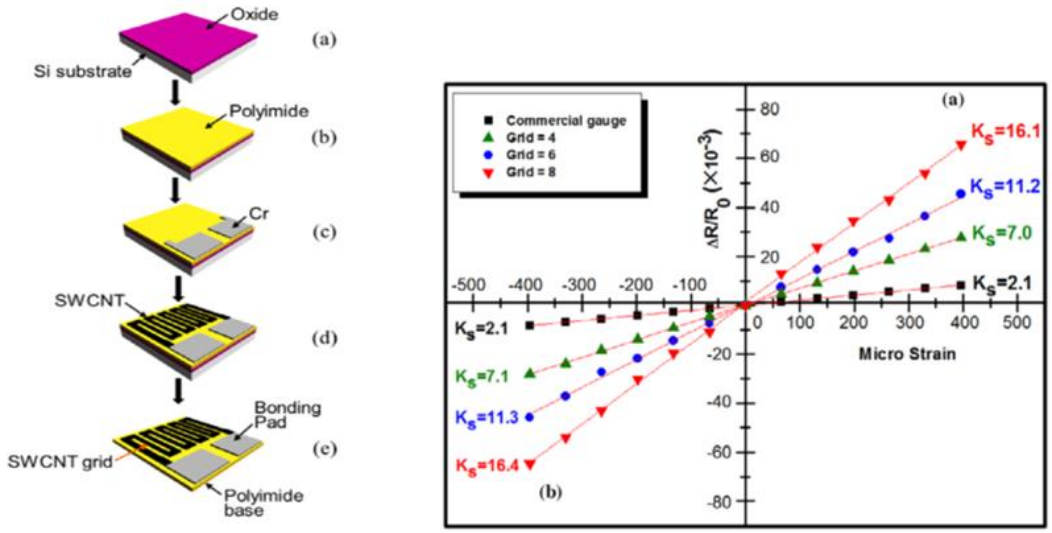

Figure 18. SWCNT serpentine pattern strain gauge fabrication process. (a)Oxide deposits on Si substrate (b)Apply polyimide on oxide surface (c)Deposit Cr on polyimide surface (d)Spray coating SWCNT and patterning SWCNT (e) Release strain gauge from substrate (left); resistance-strain relationship under tension and compression (right) (Lee et al., 2011).

Huang et al. reported a novel method to optimize CNT-based strain sensor sensitivity. They found out the sensitivity of CNT strain sensor is related to CNT growth time and line width of serpentine pattern (figure 19). They reported that 10 min growth CNT has higher gauge factor than 20 min, and gauge factor will increase if line width of serpentine pattern is thinner (Huang, Huang, Hsu, Chao, & Vu, 2012).

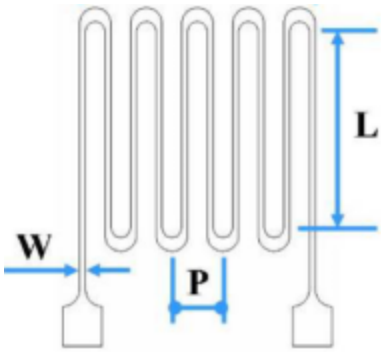

Figure 19. CNT strain sensor serpentine pattern (Huang et al., 2012).

In Lin et al.'s study, they used UV laser cutter to etching CNTs which were coated on the surface of PET film (Lin, Lin, & Li, 2010). It could ablate CNTs completely and with low residual recast material on the ablated line.

Another method used to pattern CNT thin films is spatially-modulated pulsed laser beam. SWCNTs were solution-deposited on borosilicate glass substrate. A beam of pulsed laser illuminated the backside of the glass before coming in contact with the CNT film. The optimum pulsed energy was 60mJ, as shown in figure 20, and the etched part is clear without any residual CNTs left and the etching edge was clear and sharp (Joo & Lee, 2012).

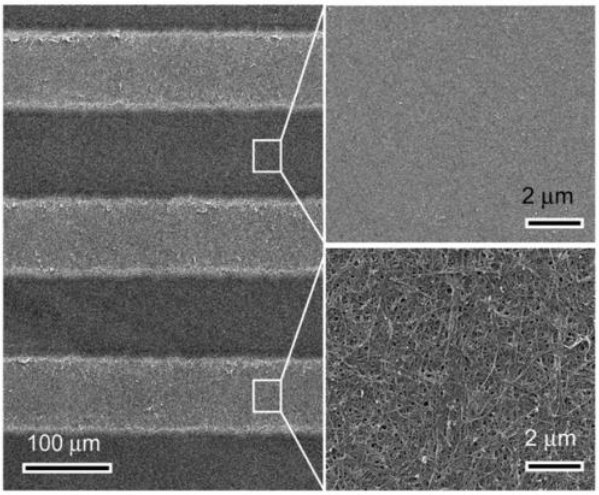

Figure 20. SEM images of etched and un-etched part under 60 mJ pulsed energy(Joo & Lee, 2012).

The reactive-ion etching (RIE) technique was used to pattern CNT strain sensors in a study by Huang et al.. RIE is a dry etching process which can generate reactive plasma to remove material from the wafer surface (Huang et al., 2012). The etched material was then be removed by the vacuum pump system.

A lot of studies have been completed to fabricate CNT/polymer thin film strain sensors to achieve high sensing performance. The process for embedding or mixing CNTs into polymer usually has sonication step involved which has high shear force will degrade CNTs properties and could impart contamination. In addition most of those processes have a lot of steps involved which consume time and energy. Thus, there is a motivation to come up with a more simple and easy method to embed CNTs into polymer and to preserve CNT properties in fabrication steps. For patterning CNT/polymer thin film strain sensors, different etching techniques have been applied to get better performance. Again, those processes introduced in literature could be complicated. Therefore, our research will focus on a novel way to etch a pattern of aligned CNTs on polymer surface. In the etching process, one of the most critical factors we will focus on is adjusting etching parameters so that the etched CNT/polymer areas stay transparent and do not become hazy. The final patterned specimen should perform with high strain sensitivity and high transparency. We will also determine if the patterning process that we demonstrate is useful for other devices in addition to strain sensors.

3 Experimental

3.1 Materials

3.1.1 Poly (methyl methacrylate) (PMMA) Film

Amorphous thermoplastic PMMA film was provided by Evonik Cyro LLC with two different thicknesses: ACRYLITE 0F016 was 60 microns, and ACRYLITE 99524 was 175 microns. Both of them were high impact modified acrylics and highly transparent (92% transmission, <1% haze).

3.1.2 Glycol-modified Polyethylene terephthalate (PETG) Film

The glycol-modified PETG film with 101 microns thickness was provided by Eastman Chemical Company. The glass transition temperature of this PETG polymer was 85℃ and transmittance was 91%.

3.1.3 Carbon nanotube array synthesized by CVD

The method used to synthesize drawable CNT array was chemical vapor deposition (CVD). One gram $FeCl_2$ catalyst was added in a boat and then placed the boat inside of the secondary quartz tube along with quartz substrates for CNT growth. Then the secondary quartz tube was transferred slowly all the way inside of the furnace. The chamber was pumped to around 6 mTorr, and after that, the temperature program was initiated to raise the temperature to 760℃. After the temperature reached 760℃, acetylene, chlorine and nitrogen switches were

opened to flow gases into the chamber. In this process, 600 sccm acetylene, 400sccm argon and 1.5sccm chlorine were used. At this point the growth time was recorded. After 10 minutes the acetylene was shut off while the other gases were used to conduct a post treatment at the same temperature for 20 minutes.

After 10 minutes growth and 20 minutes post-treatment, the furnace was turned off. After it cooled down to about room temperature, the inner quartz tube was removed carefully and placed on a holder in a fume hood. Then the substrate with CNT growth on was removed from the tube. The CNT sheet could be drawn from the CNT array by a tweezer or razor blade.

3.2 Sample Preparation

3.2.1 CNT/PMMA or PETG film fabrication

To fabricate the CNT/PMMA thin film, a drawable CNT array, a piece of 3×5 inch PMMA film, two metal plates and a Wabash hydraulic press were used. First, a clean room wiper soaked in ethanol was applied on the metal plates and the PMMA film surface to remove any potential contamination. Then the CNT sheet was stretched by a tweezer or a piece of tape from the drawable CNT array across the metal plate as shown in figure 21. Since the MWCNTs array synthesized in our lab had strong Van der Waals interaction with each other, they could be easily stretched into a horizontal CNT sheet. The CNT sheet was semi-transparent and lightweight. In our preliminary experiments, we found out that the resistance

of one layer CNT embedded into polymer film was quite high, which may be not suitable for real life application. In order to solve this problem, we applied two layers of the CNT sheet to be embedded in the surface of the polymer. In some of the sample these two layers of CNT were in the same direction, but in another set of sample the second layer was perpendicular to the first layer CNT, which is referred to as cross-ply CNT/polymer thin films. Next the piece of PMMA film was placed on the CNT sheet carefully, because it was easily to cause the CNT sheet to bundle when handled roughly. The other metal plate was applied on top. The whole setup was transferred to the Wabash hydraulic press carefully (Wabash Metal Products Company, INC.) which applied heat and pressure to sample (figure 21(d)). Different temperature, time and pressure settings were attempted in order to find a good way to fully embed CNT into PMMA. After many trials, we found out the optimum temperature and pressure to embed CNT in PMMA was 135 ℃ and 2 tons of force respectively for 10 minutes. The heat press was turned on and the temperature was set up to 135 ℃. The sample was transferred to it after the temperature reached 135℃ and then the pressure was increased up to 2 tons. After 10 minutes heating, the heat press was turned off and the sample was left in the hot press to cool down to room temperature under 2 tons pressure. This was done because the film started to develop wrinkles if the pressure was released right after heating. The water cooling system on the heat press was used to increase the cooling rate.

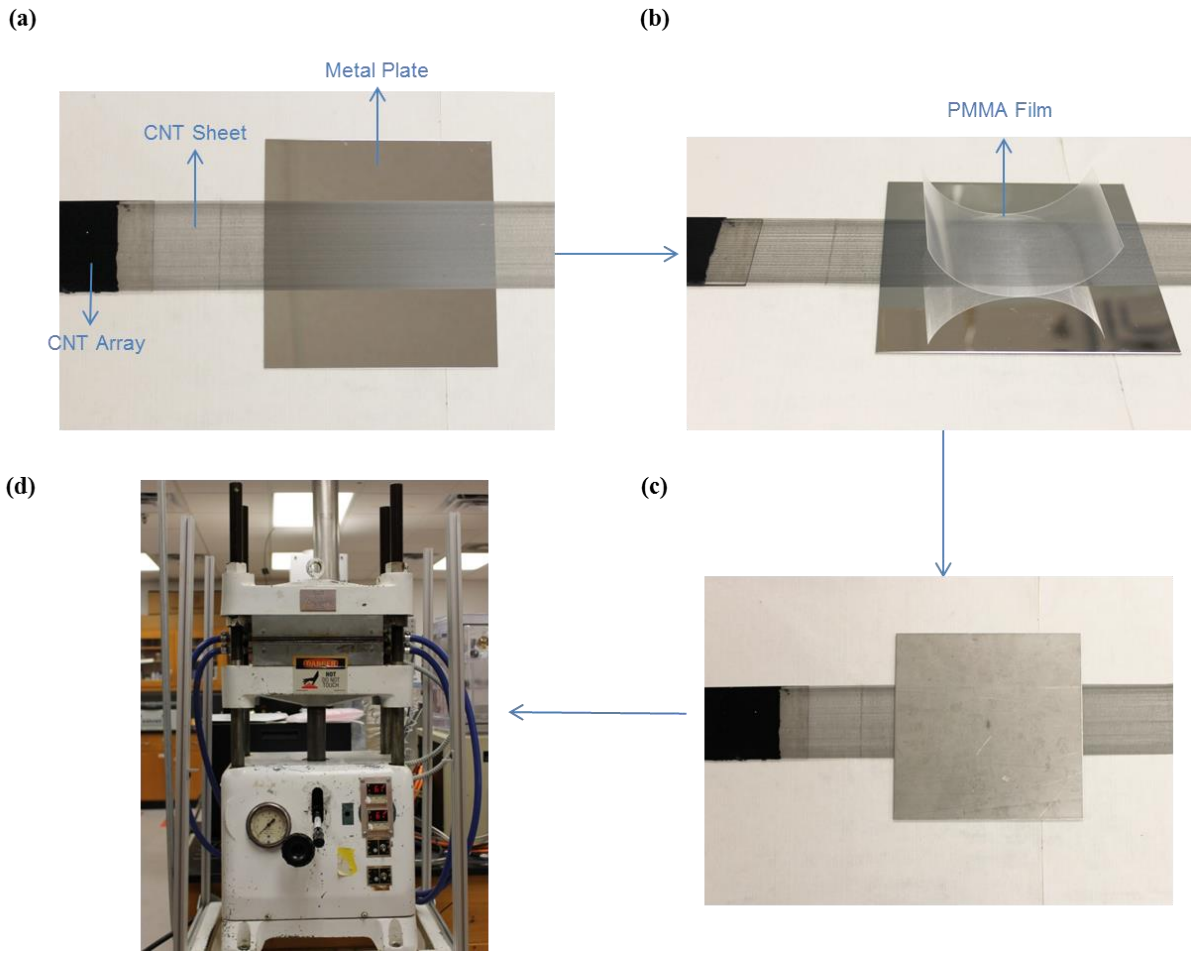

Figure 21. Embedding aligned CNT sheets into PMMA films.(a) Stretch CNT sheet across metal plate; (b) Apply polymer film on top of CNT sheet; (c) Apply another piece of metal plate on top; (d) Transfer to Wabash hydraulic press.

However, in this study, for PETG, there was no optimal parameter found in heat press because air bubbles kept showing in the PETG film during heating which hindered CNT from fully embedding. Another alternative way for fabricating CNT/PETG thin film was a calendar system (Figure 22).

After many trials were performed in calendar system, the optimum temperature for fabricating CNT/PETG film was 135℃ as well. After temperature of the calendar was raised to 135℃, a piece of teflon with high temperature adhesive backing was carefully applied on the calendar in order to prevent the CNT sheet from sticking to the rollers. If the teflon was applied to the calendar rollers at room temperature then heated, air bubbles would appear in teflon because of thermal expansion, which would cause wrinkles to be formed in the PETG film. PETG film from the front mandrel went through two tension rods and then inserted into the gap between two middle calendar rollers. The CNT sheet was stretched from array and then applied to the PETG film right in front of the middle calendar. When the motor was turned on, the CNT/PETG film would transfer along with the rotating calendar at a speed of 0.57 m/min. The final CNT/PETG film was then collected by the take up mandrel.

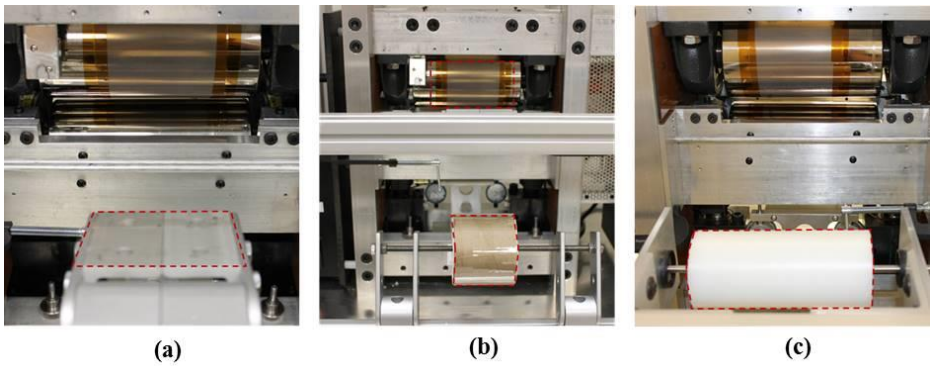

Figure 22. Calendar system. (a) Front view with CNT array holder; (b) Front view with PETG film mandrel; upper calendar provides heat and pressure; (c) Back view with mandrel for collecting CNT/PETG film.

3.2.2 Transmittance measurement

Varian Cary 300 UV-Vis Spectrophotometer with UV-Vis range from 800 nm to 200nm was used to quantify the transmittance of the CNT/polymer thin film. The sphere attachment was installed to measure transmittance. Baseline correction was completed before each measurement.

3.2.3 Sheet Resistance measurement

A four point probe method was used for measuring the CNT/polymer sheet resistance in this study. Current (Keithley 6221) was passed through the outer two probes and voltage (Keithley Model 2182A) was measured by inner two probes (Figure 23). The voltage ranged from 10 mv to 10v at 1 µA current. Therefore, the sheet resistance measurement limit was 10 Mohms. The main purpose of this current and voltage separation design is to eliminate contact resistance from measurement.

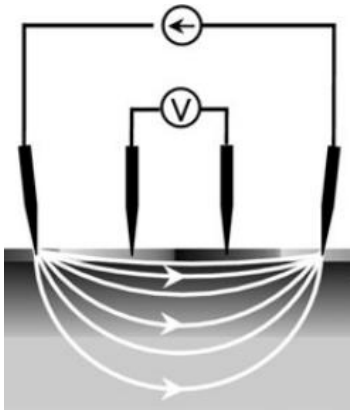

Figure 23. Schematic of four point probe for sheet resistance measurement (Hasegawa et al., 2002).

3.2.4 Etching pattern by laser cutter

A laser cutter (Legend Laser Series, Epiloglaser, USA) was used to cut or etch samples in this study (Figure 24). Cutting and etching power, speed, frequency and focus position could be set up in the Coreldraw software in the computer which is connected to laser cutter. Maximum speed and power of this laser cutter were 80 ips and 40 watt respectively. The PMMA used in this study had a protective film which was removed before cutting or etching. Nitrogen was used as a protective gas for cutting to prevent charring and fire.

Figure 24. Computer controlled laser cutter.

When the laser beam came across the working surface, the temperature of irradiated spot increased significantly which caused CNTs and PMMA on the very surface to ablate. PMMA is an ideal material to use as a substrate in this study because for the most part it vaporizes

instead of melting, when exposed to the laser. This allows for much cleaner cuts and etching than most thermoplastics.

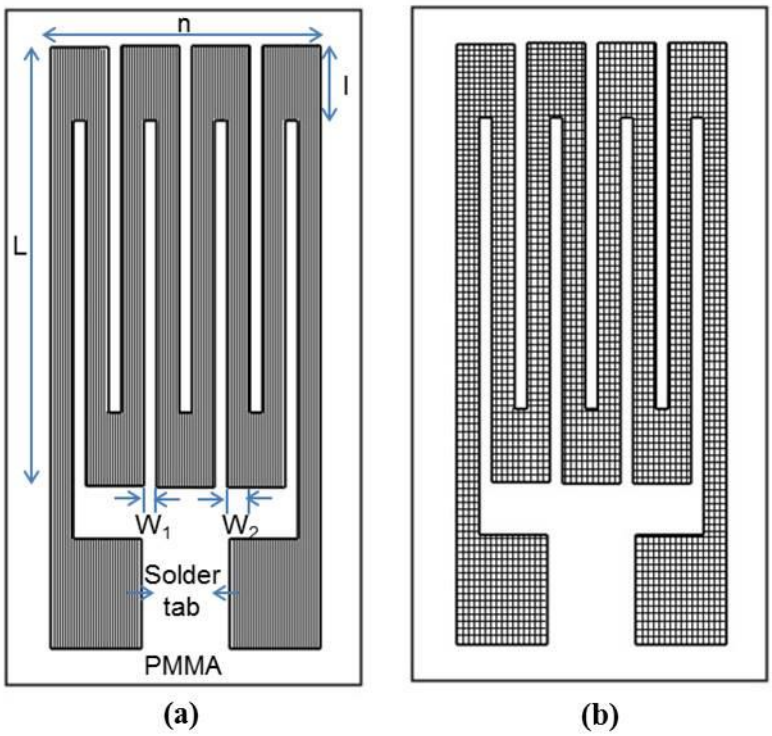

Figure 25. Schematic of serpentine pattern. The white area is insulating backing material (PMMA). The dark area is embedded with CNT. n: number of grids=1, 2, 4, 6, 8, 10; L: Active grid length=30mm; W_1: gap between two adjacent grips=0.83mm; W_2: width of grips=1.5mm; l: end loop length=5.1mm. (a) Double layers CNT embedded into PMMA (b) Cross-ply layers CNT embedded into PMMA.

To obtain nicely cut or etched samples, the user must know how the speed, power and focus position change the cutting/etching behavior. Focus position was the height at which the laser spot size was the smallest on the working surface. In this study, the distance was always

determined by auto-focus operation of the device. The process for determining the optimum etching parameters will be discussed in the next chapter. The etching pattern design is shown in figure 25. The dimension for double layer CNT/PMMA thin films and cross-ply CNT/PMMA thin films was same. The CNTs could be totally etched after laser beam etching and then CNT fragments and decomposition products from etching were gently wiped off with ethonal.

3.2.5 Coupon Preparation

Two different kinds of coupon were used in this study. One was glassfiber composites made from pre-impregnated fabrics (Prepreg 7781 E-Glass, Fibre Glast Developments Corp, USA) and another was acrylic which could provide high transparency. The method to prepare glassfiber prepreg composites was vacuum bagging. Figure 26 shows the vacuum bagging layup. After every layer was positioned, the vacuum bag was sealed on the edge with sealant. A vacuum pump was applied to remove the trapped air within the vacuum bag. Then the whole setup was transferred to hot press carefully. Temperature was set up to 290ºF and the panels were cured for two hours on the hot press. After two hours, the prepreg became a stiff and flat composite panel. Then this composite panel was cut into desirable dimension coupons (295mm×24mm×1.9mm) by wet diamond saw. To make the acrylic coupons the acrylic sheet was cut into a dogbone shape in laser cutter. The power and speed were used to cut through 6mm thick acrylic are 65% and 3% respectively. The cutting edge was very smooth and clear as shown in figure 28. However, the honeycone shape of vector cutting

table in laser cutter reflected on the surface of acrylic during cutting which damaged the bottom side. A couple layers of paper were placed underneath the piece of acrylic to minimize this damage. The dog-bone shape helped to avoid stress concentration on the two ends of coupon when applying stress in the tensile test.

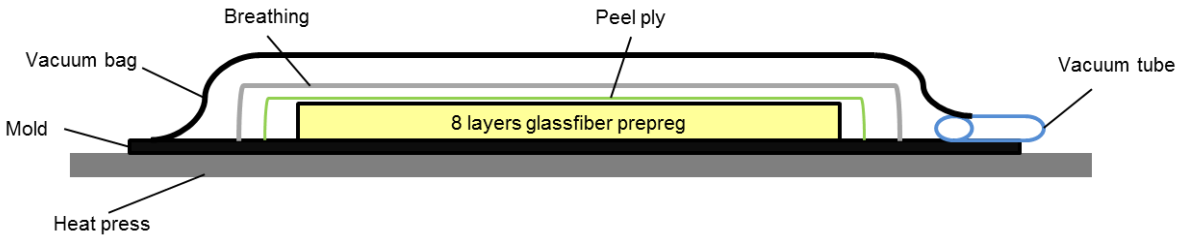

Figure 26. Diagram of VARTM layup.

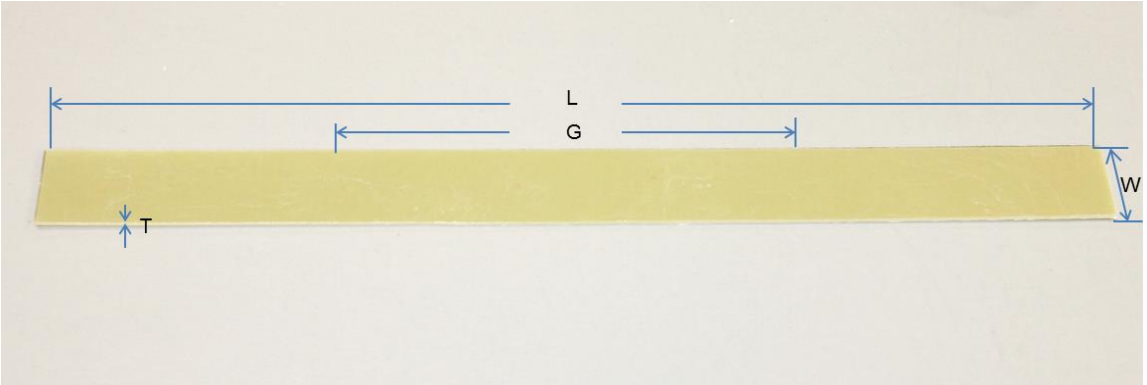

Figure 27. Glassfiber prepreg composites coupon. L: Length overall = 295mm; W:Width=24mm; T: Thickness=1.9mm; G: Gauge length=145mm.

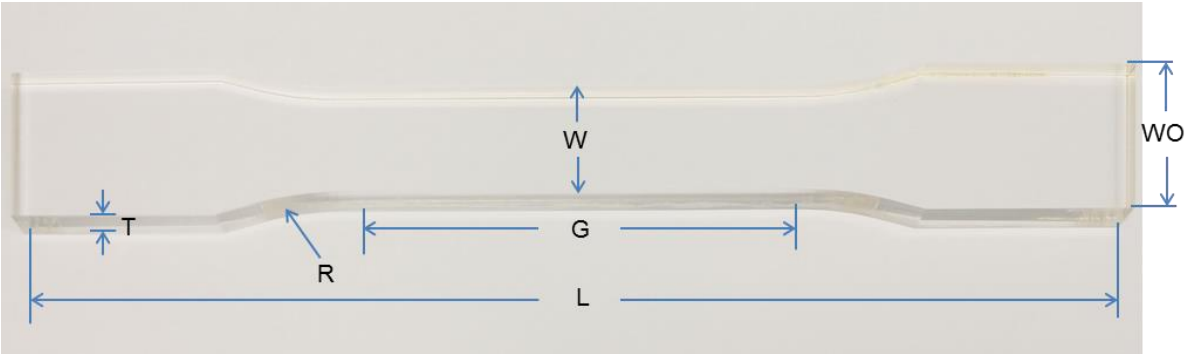

Figure 28. Dogbone shape acrylic coupon. W: Width of narrow section=25.4mm; WO: Width overall=35.56mm; G: Gauge length=88.90mm; T: Thickness=6mm; R: Radius of fillet; L: Length overall=267mm.

3.2.6 Mounting Specimen and Strain Gauges on Coupons

The fabrication process for mounting CNT/polymer thin film and commercial metal-foil strain gauge (Vishay Micro-Measurement 250LW, USA) on glassfiber prepreg composites or acrylic coupons is summarized as follows. First, after fabricating the CNT/ polymer thin film, the film was etched into the desired pattern and cut into the desired outer dimensions by laser cutter. Then two pieces of metal foil with 5 mm×10mm dimension were attached to the two electrodes by silver epoxy. The preparation of the coupon surface was very crucial to ensure good bonding between the sample and metal-foil strain gauge on the coupon. All surface preparation materials were purchased from Micro-Measurement. First, CSM-2 degreaser was applied on the surface of coupon uniformly with gauze sponge. Moderate amount of M-PREP conditioner A was dropped on the middle part of the coupon which followed by sanding with a small piece of sand paper (220 grit silicon-carbide paper) in order to create rough surface for adhering the sample, then followed by wiping off all glassfiber fragments

with a gauze sponge. The same amount of M-PREP neutralizer 5A was used with a cotton-tipped applicator to neutralize the surface. Then M-Bond 200 catalyst-C was applied on sample surface for faster adhesive hardening. Finally several drops of M-Bond 200 adhesive were applied on the coupon surface, and then the CNT/polymer sensors were applied on top of the adhesive immediately. Then temperature and pressure provided by a finger were applied on the sample for about two minutes until the adhesive hardened totally. After the adhesive cured, the commercial metal-foil strain gauge was mounted on the opposite side of coupon surface by repeating the above steps. One extra step was applying M-Coat polyurethane protective coating on the surface of the metal-foil strain gauges. Commercial metal-foil strain gauges were used here to collect accurate strain data for sensor calibration. Two wires were attached on each of metal foil pieces surface by Ag solder. The finished specimen is shown in figure 29.

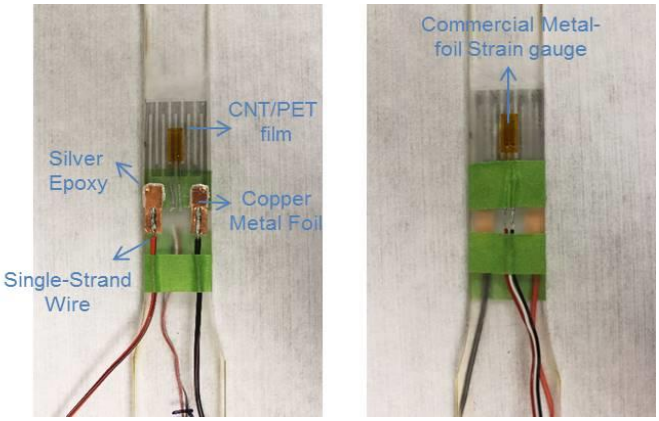

Figure 29. Fabricated CNT/PMMA strain sensor mounting on acrylic (left); commercial metal-foil strain gauge mounting on acrylic (right).

3.2.7 MTS Landmark Servohydraulic Test System for Tensile Testing

The tensile test machine has been used in this study was MTS Landmark Servohydraulic Test System (MTS, USA). One crucial step before start testing was making sure two grips were well-aligned in order to avoid any misalignment during testing so that the test data was accurate and reliable. The lower grip was fixed for holding sample in the standard position, and the upper grip applying tensile stress on the specimen (Figure 31). The strain data during tensile test was collected by a strain gauge reader. The resistance was measured by a 34410A $6\frac{1}{2}$ digital multimeter (Figure 30).

Figure 30. Aglient 34410A 61/2 digital multimeter.

In order to optimize resistance measurement and minimize the contact resistance between leads and two solder tabs, four probe resistance measurement was applied to measure resistance during the whole experiment. The real-time resistance change was recorded by

BV0001A BenchVue Digital Multimeter Pro software. The tensile test speed was 1.5mm/min. The strain data collection and resistance measurement were launched together and also ended at the same time right after the specimen fracture. The time interval for both strain data and resistance data collection was 0.1s.

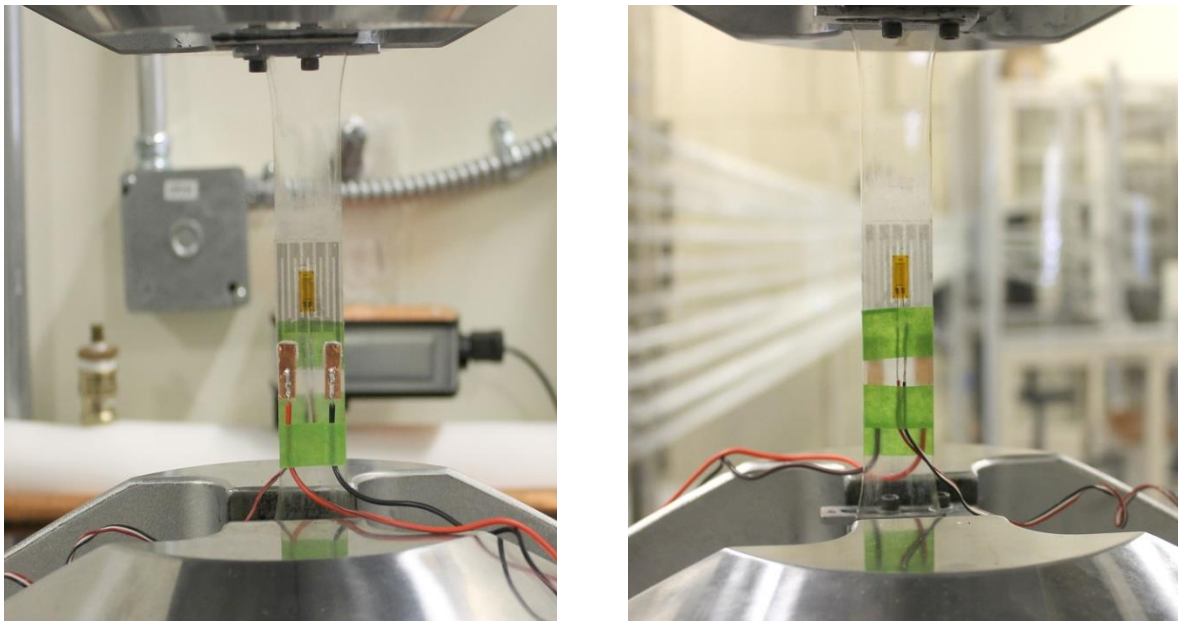

Figure 31. Specimen is clamped by MTS Landmark Servohydraulic Test System.

4 Results and Discussion

4.1 Etching power and speed

When the laser cut or etched the specimen, nitrogen usually worked as a protective gas in case of fire or flame. In the preliminary work, different etching powers and speeds were attempted in laser cutter with nitrogen on to find out the optimum way to etch CNTs out without increasing polymer surface roughness. The etching powers tried were 3%, 5%, 7%, 9%, 11%, and 13% at 50 % speed on the double layer CNT/PMMA thin films.

The results of different etching powers are shown in figure 32. For 3% etching power, the laser barely etched any CNTs off the surface because the power was not strong enough. Above etching power of 5%, a fraction of CNTs was etched at 7% and 9% power; while all CNTs were etched out of the surface at 5%, 11% and 13% power. The background could be seen most clearly without haze at 5% and 13% power. However, the surface roughness increased with the etching power, which has potential to impair the surface performance. It could be proven in figure 33, the distance between film and background picture was approximately a half meter. The background picture was shown clearly at 5% etching power. However, for 13% etching power, the haziness of the etching part increased a lot, so that the background picture could not be seen at all. The problem was that the 13% etching power was fairly strong, so that it made the PMMA surface more rough and cloudy. Above 7% etching power, the etched part became fragile and cracks started form because the engraving depth increased with power, which caused the PMMA film to be more fragile and brittle. To

relieve the residual stress, annealing was done right after every sample was etched and cut. The etched sample was put into the oven at room temperature then heated it up to 80 ℃. The whole process was around two hours. We left the sample in the oven and waited until it cooled down to room temperature. The cooling rate did not exceed 15 ℃ per hour. After annealing, the sample was flat and less prone to cracking.

Figure 32. Visual transparency comparison under different etching powers.

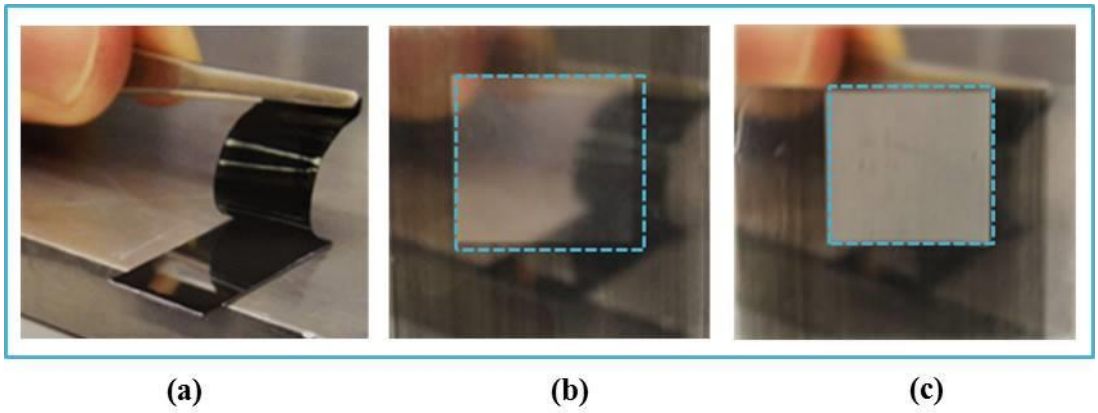

Figure 33 Remote visual transparency comparison. (a) original picture; (b) 5% etching power; (c) 13% etching power.

The transmittance of each etched part was measured by a Varian Cary 300 UV-VIS spectrophotometer. The transmittance result is shown in figure 34. For 5%, 11% and 13% etching power, the transmittance shows better results than other etching powers at 550 nm wavelength, which is in accordance with the result shown in figure 32. The transmittance of 11% and 13% etching power went back up because so much material has been etched away, even if it is cloudier.

From the preliminary work, 7% and 9% powers showed unexpected etching results, where only part of the CNTs were etched even though even lower powers could fully etch the surface. It was suspected that the CNTs were not being fully etched because they were being etched in a nitrogen atmosphere. To verify this, two CNT/PMMA films were etched with and without nitrogen respectively. We found that the specimen had better transmittance without

nitrogen (Figure 35). Based on those results, we turned off nitrogen when etching and turned it on only when cutting.

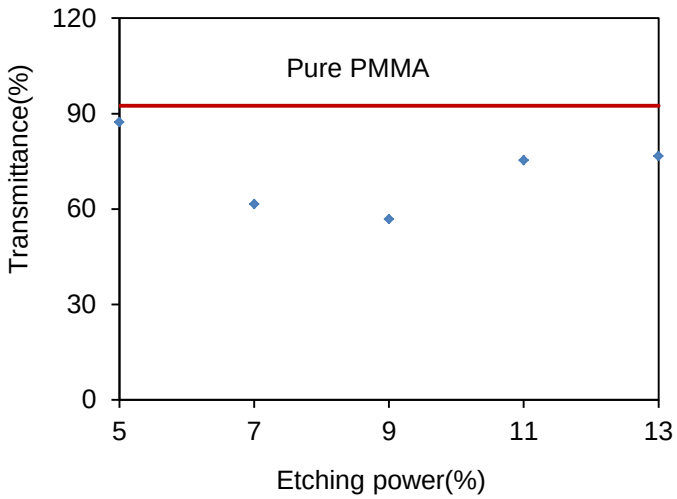

Figure 34. UV-Vis spectroscopy results from different etching powers.

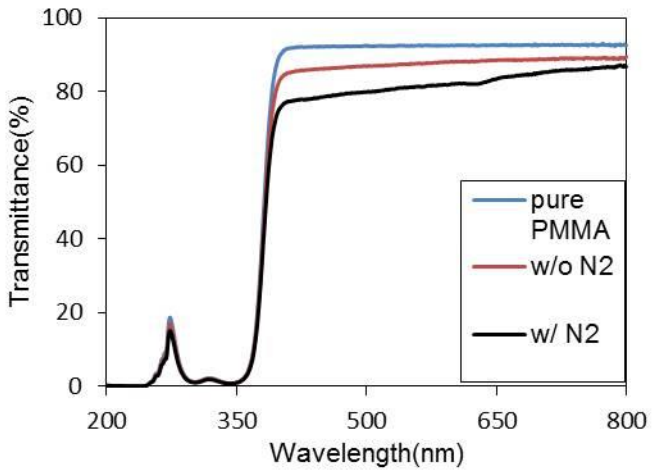

Figure 35. Transmittance results of specimen etched with and without Nitrogen.

After we found out the best result from the preliminary work, the correlation between etching speed and power was studied more closely on both double and single layers CNT/PMMA films. The power changed from 2% to 8% with 1% increase each time and the speed changed from 25% to 50% to 75%. The sheet resistance and transmittance of each etching part is shown in figure 36. For double layers CNT/PMMA films, under 75%, 50% and 25% speed, the resistance went to infinity after 7%, 5% and 4% power respectively; while for a single layer, the resistance went to infinity after 6%, 5%, 3% power respectively. The CNT films were considered to be completely removed if the resistance of etched part was higher than 20 MΩ (Lin et al., 2010). That was the most straightforward way to judge if CNT was totally etched out of the surface. Transmittance of both films showed the same trend that increased first and then decreased, which proved that CNTs were gradually engraved out of surface by increasing power, but after certain point, the surface roughness increased with etching power. Overall, the transmittance of single layer CNT/PMMA films was higher than double layers one.

After finding out that 5% power and 50% speed were good etching parameters, a deeper study was carried out to find the best etching speed, to provide the CNT/PMMA film even higher transparency. This test was carried out on single and double layer CNT/PMMA films as well. In the last trial, CNTs were totally etched at 50% speed but still had lots of CNTs left at 75% speed; so for this test, the speed was chosen between 50% and 76% with increase 2%

each time. The sheet resistance went to infinity from 50% to 60% and 62%, which indicated CNTs were etched completely. However, some etched places still had CNTs left, as shown in figure 37, because laser cutter etched the very surface layer of CNTs and a thin layer of polymer covered the CNTs underneath. As a result, the four point probes could not reach the CNTs underneath the thin layer of polymer. 50% etching speed still showed the highest transmittance in both films.

Better transmittance was achieved from the single layer CNT/PMMA thin films. However, it had much higher sheet resistance. With more CNTs embedded into the PMMA, more light was absorbed, which resulted in lower transmittance. However, more CNT layers also created more conductive paths which lowered the overall resistance.

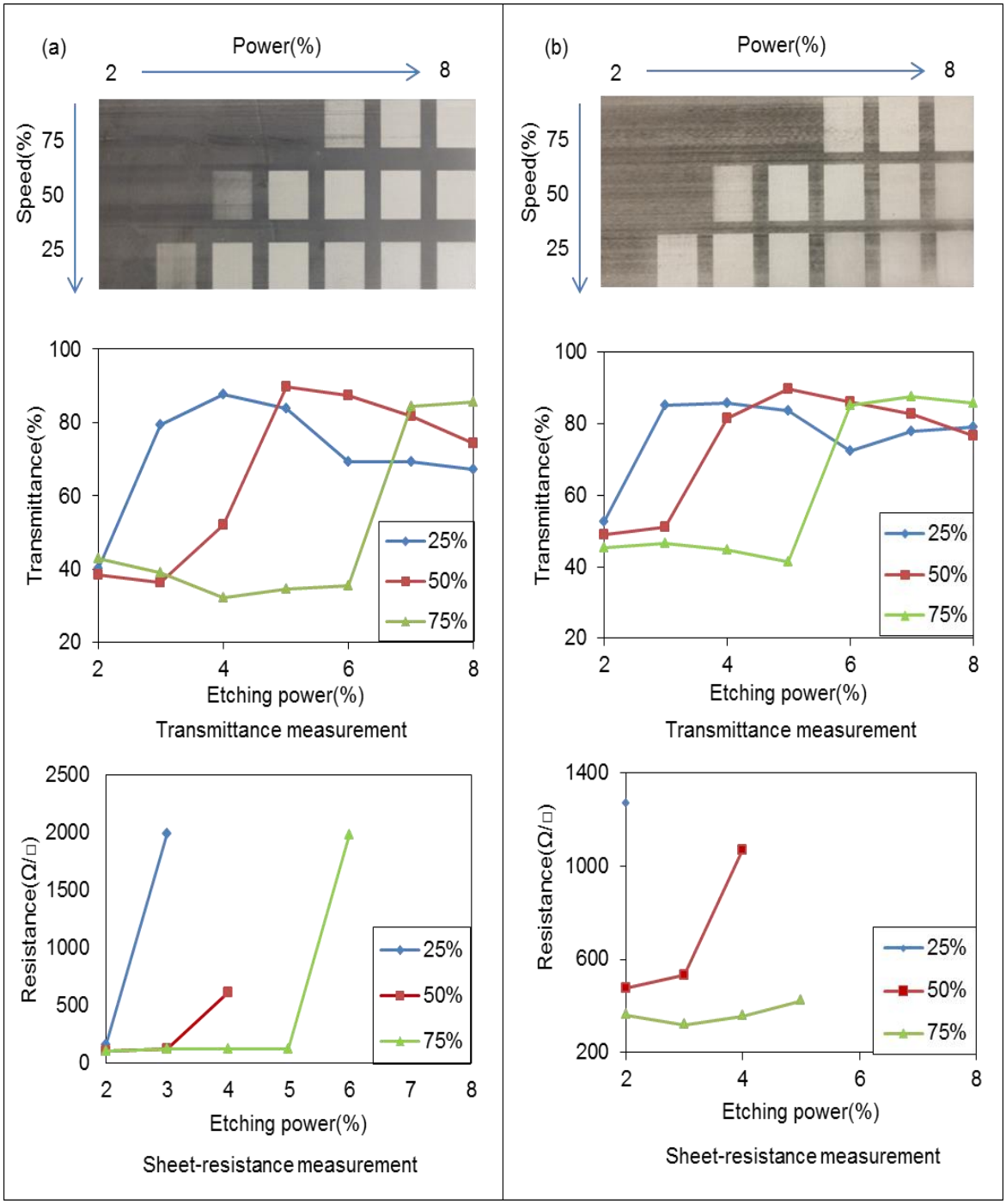

Figure 36. Changing etching speed by decreasing 25% each time from 75% to 25% and power by increasing 1% each time from 2% to 8%. (a) double layers CNT/PMMA film; (b) single layer CNT/PMMA film.

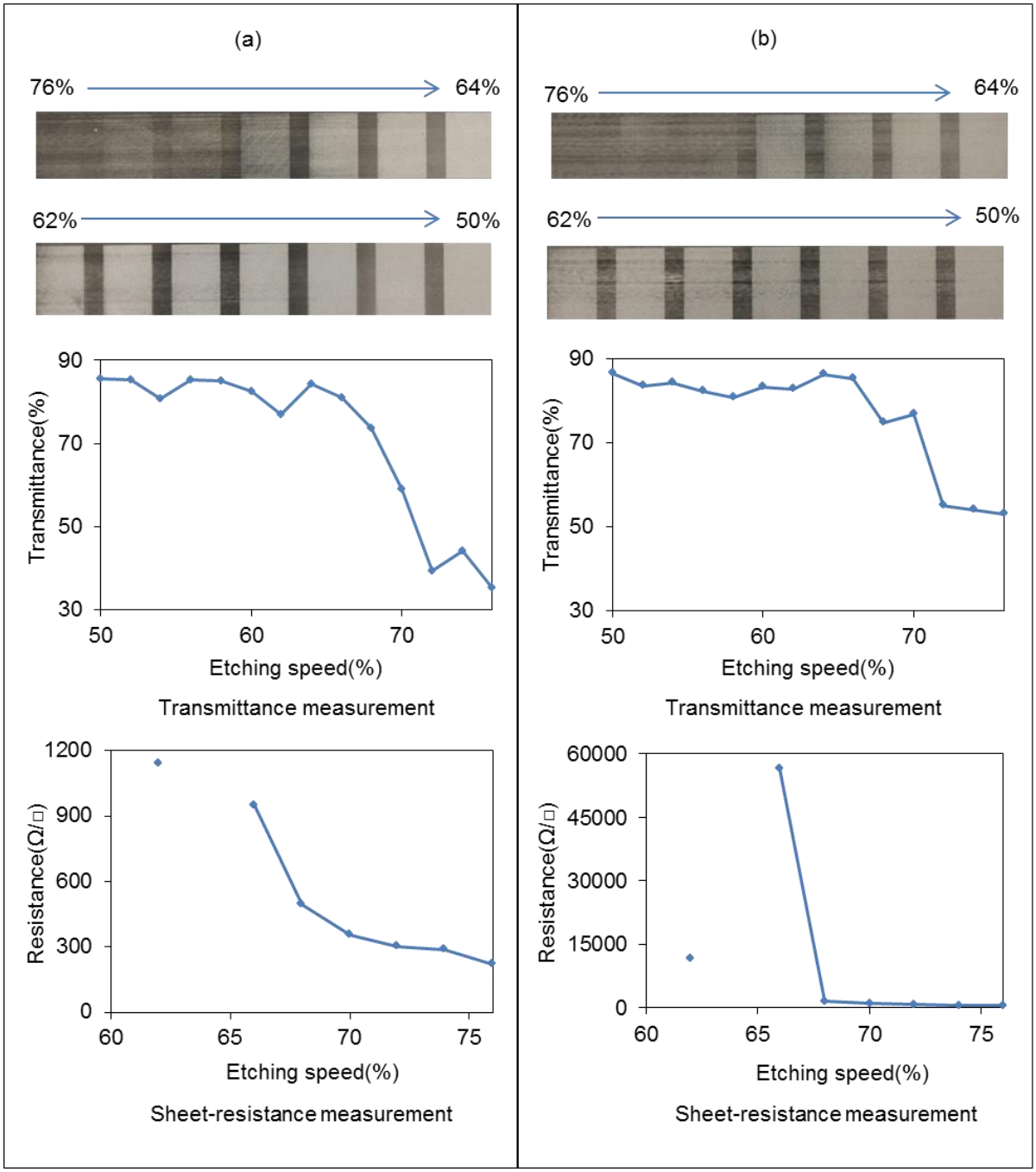

Figure 37. Changing etching speed by decreasing 2% each time from 76% to 50% under 5% power. (a) double layers CNT/PMMA film; (b) single layer CNT/PMMA film.

The surface morphology of both double layer and cross-ply CNT/PMMA thin films was observed under a Field Emission Scanning Electron Microscopy (FESEM)-Verios. Both samples were coated with gold in order to get high quality images. As shown in figure 38, the left part was the etched area and right part was the non-etched area. The etched area still had a few CNT fragments left but were separate from each other. Therefore, this part of the film acted as an electrical insulator. The etching edge was sharp and clear, which indicates 5% power and 50% speed were good etching parameters. Figure 38(b) shows a lower magnification image of the etched and non-etched areas of a cross-ply sample.

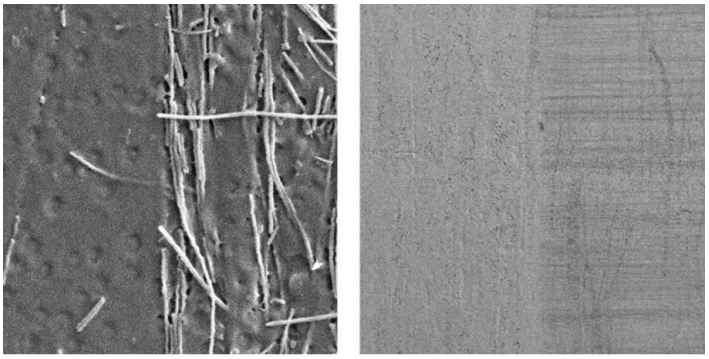

(a) (b)

Figure 38. Surface morphology images under FESEM-Verios. (a) double layers; (b) crossply layers CNT/PMMA thin film.

4.2 Quasi-Static Monotonic Tensile test procedure and results

As mentioned in the literature review, the resistance of CNT/ polymer thin films changes under axial tensile strain, which can be attributed to three aspects: (1) the change of the

intrinsic piezoresistivity of CNTs; (2) contact resistance between CNTs; (3) tunneling effect between CNT in close proximity but not touching. In CNT/polymer thin films, there are three main load transfer mechanisms operating between the CNTs and polymer during tensile loading. The primary one is Van der Waal force between CNTs and polymer. The second one is micromechanical interlocking which is hard to implement in the CNT/polymer films case because of CNT's smooth surface. The third one is covalent or ionic bonding between CNTs and polymer, which is also the most desirable mechanism. This mechanism could be achieved by surface treatment of CNTs, such as oxidation (Choudhary et al., 2013).

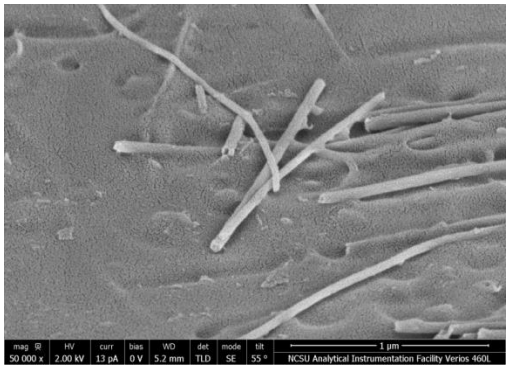

Figure 39. The SEM image shows the surface of CNTs.

Since the surface of CNTs synthesized in our lab is very smooth (Figure 39), and we did not do any special surface treatment on CNTs, the primary loading transfer mechanism between CNTs and polymer is Van der Waal force.

The first factor that we focused on was the influence of the number of active grids on resistance change of our etched sensors. The serpentine pattern we used in our study consisted of multiple active grids, so that a strain change resulted in much larger resistance change when the stress was applied in the direction of parallel to the grids than only one straight active grid. Therefore, we hypothesized that the magnitude of resistance change would increase with the number of active grids.

During tensile loading, acrylic coupons showed large variations in the failure strain ranging from 0.8% to 1.8%. The resistance change corresponded to strain was irregular. Therefore, the tensile test results were not reliable. However, the glassfiber prepreg composite coupons always showed reliable and stable failure strain values during tensile loading, which was around 2%. While the acrylic samples allowed us to show the semi-transparent nature of our sensors, the tensile test results shown below were all acquired using glassfiber prepreg composite coupons. An example of the tensile tests conducted on acrylic coupons is located in the Appendix. All tensile tests were carried out under room temperature and ambient atmosphere.

The initial resistances of the sensors with different number of grids are listed in Table 1. The electro-mechanical properties of serpentine pattern based double layers CNT/ PMMA strain sensors are shown in figure 40.

Table 1. Initial resistance of different number grids sensor (double layers CNT).

Grid	1	2	4	6	8	10
Resistance (kΩ)	4.32	12.76	19.57	27.95	39.93	46.53

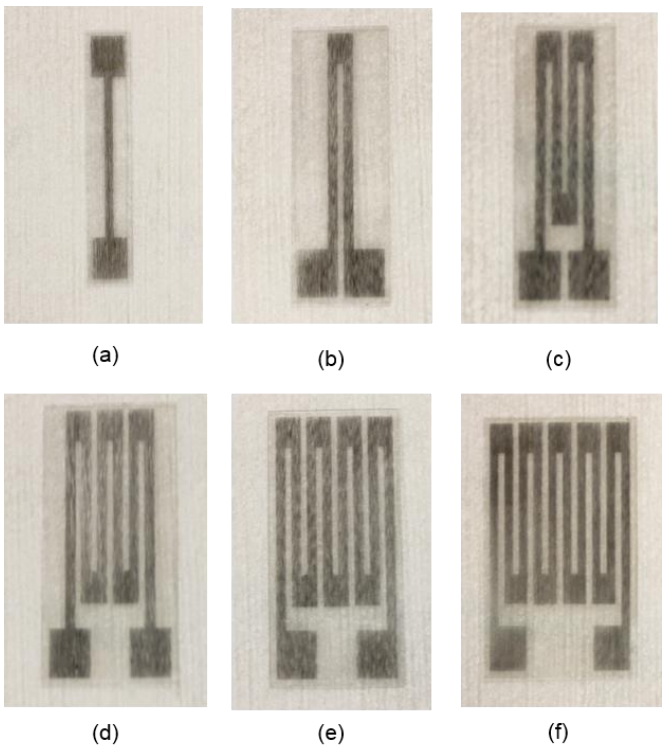

Figure 40. Sensors with increasing number of grids. (a)1 grid; (b)2 grids; (c)4 grids; (d)6 grids; (e)8 grids; (f)10 grids.

Overall, the responses of both the magnitude of resistance (ΔR) to ε and the normalized resistance change ($\Delta R/R_0$) to ε showed non-linear behavior. In the experimental results, ΔR vs. ε and $\Delta R/R_0$ vs. ε showed tradeoff trends. The magnitude of resistance change increased

with the number of grids except 10 grids pattern as shown in figure 41. However, the nominal resistance change ($\Delta R/R_0$) decreased with increasing the number of grids.

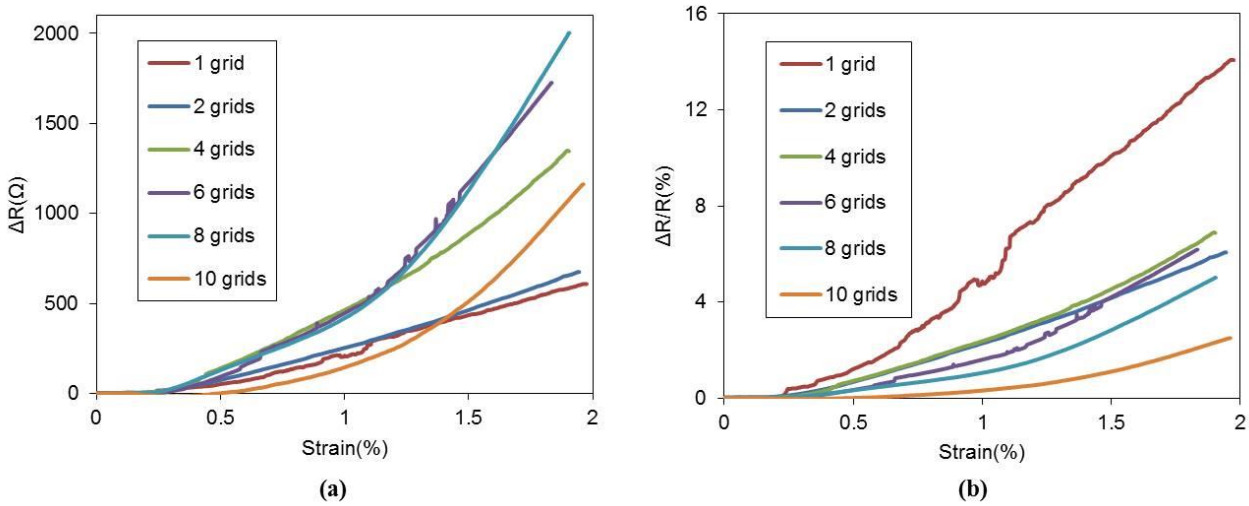

Figure 41. Electromechanical results for double layer CNT/PMMA sensors. (a) in situ resistance change for increasing number of grids during tensile testing; (b) in situ nominal resistance change for increasing number of grids during tensile testing.

As shown in figure 41, at low strain levels (0 – 0.3%), the curve exhibited quasi-linear behavior with almost zero change in resistance. It was observed that an increase in resistance occurred at around 0.3%; the curve typically became even steeper around the strain of 1.5%. The magnitude of resistance change increased with the number of active grids, which was consistent with our hypothesis. The tensile loading applied in the direction of parallel lines made the active grids thinner and longer, with sensors with more active grids having a longer effective length. However, the normalized resistance change decreased due to the increase in

initial resistance with the number of active grids. Therefore there was tradeoff trend between magnitude of resistance change and normalized resistance change (figure 42).

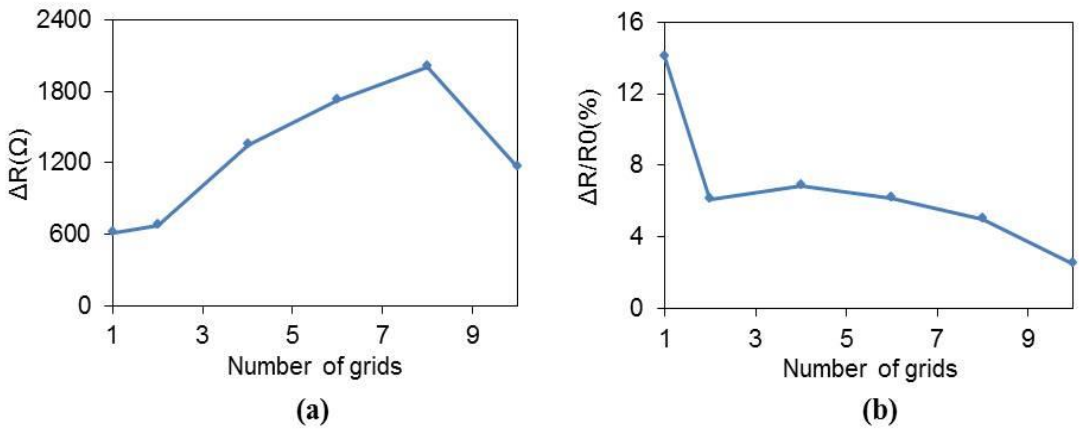

Figure 42. Double layer CNT/PMMA sensor maximum value comparison for each pattern. (a) Resistance change vs. number of grids; (b) Resistance change over initial resistance vs. number of grids.

Another series of tensile tests were conducted on cross-ply CNT/PMMA strain sensors. Cross-ply means consist of arbitrary number layers of same material and thickness but orientate in 0° and 90° alternatively (Jones, 1999). In this study, we've been using one 0° layer and another 90° layer in order to keep the consistent number of CNT sheets with previous double layer CNT samples. In double layers CNT/PMMA strain sensors, the resistance of end loops was much higher than active grids. Typically, the average resistance of an end loop was 5 kΩ. Therefore it was harder for electrons to go through these areas because they had to hop across parallel CNTs. By adding another layer of CNTs sheet which

is perpendicular to the first, the CNTs layer could more easily move electrons across the end loops, reducing the resistance in the end loop areas. After adding the cross-ply CNTs sheet, the resistance of the end loop decreased to 1 kΩ, which was a significant change. However, the total resistance didn't change too much as shown in table 2 because the resistance of active gauge grids increased because only half the CNTs were aligned in the grid direction.

Table 2. Initial resistance of different number grids sensor (cross-ply layers CNT).

Grid	1	2	4	6	8	10
Resistance (kΩ)	6.79	11.38	17.70	39.80	28.80	87.60

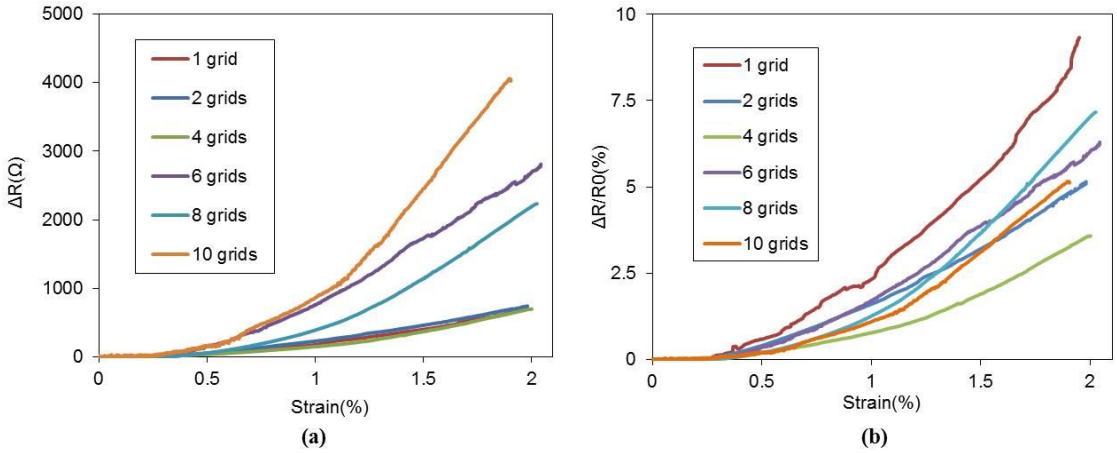

Figure 43. Electromechanical performance of cross-ply CNT/PMMA sensors. (a) in situ resistance change for increasing number of grids during tensile testing; (b) in situ nominal resistance change for increasing number of grids during tensile testing.

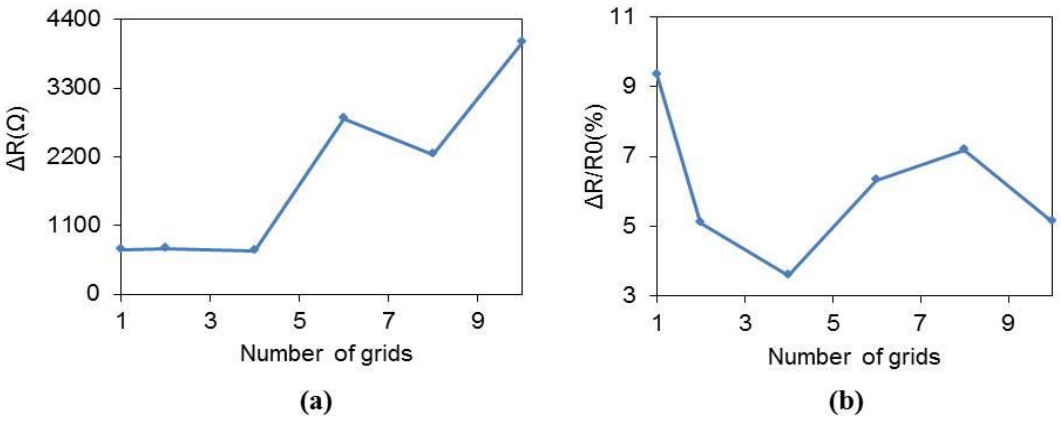

Figure 44. Cross-ply sheets CNT/PMMA maximum value comparison for each pattern. (a) Resistance change vs. number of grids; (b) Resistance change over initial resistance vs. number of grids.

For the cross-ply CNT sheets strain sensor, it didn't show an obvious resistance change trend with an increasing number of grids. However overall, in figure 43, it still shows that the overall the magnitude of resistance change increased with number of grids and the normalized resistance change decreased.

Comparing the result with double layers CNT/PMMA strain sensors, the cross-ply layers CNT/PMMA strain sensors didn't show superiority in terms of the magnitude of resistance change. However, one advantage of this cross-ply geometry is that the resistance distribution within this structure is closer to the standard of commercial metal-foil strain gauge, which is the resistance of end loop could be neglected and doesn't make contribution to the overall resistance change during tensile loading since the end loop should only play the role in connecting two active grids. Likely the best way to increase the sensitivity would be to

introduce a method to decrease the resistance in the end loops while maintaining the lower resistivity in the active grid sections. This is not covered in this work but is suggested as future work.

Based on the tensile test results from double layer and cross-ply CNT/PMMA strain sensors, the 6 grid pattern showed high total resistance change and fairly good sensitivity overall. Thus, for most following tensile tests, the 6 grid pattern was chosen.

It was also assumed that the width of active gauge grid would have an effect on the sensing performance. If the active gauge grid becomes thinner, less CNTs can carry on electrons. The electrical conductive paths become less, so that the initial resistance becomes higher. This trend is shown in table 3 as we increased the width of the grids from 0.5 mm to 2 mm. The spacing between grids was kept constant to maintain a similar resistance in the end loop area as shown in figure 45.

Table 3. Six grids pattern initial resistance with different grid width.

Grid Width(mm)	0.5	1	1.5	2
Initial Resistance(kΩ)	77.50	55.10	39.80	25.70

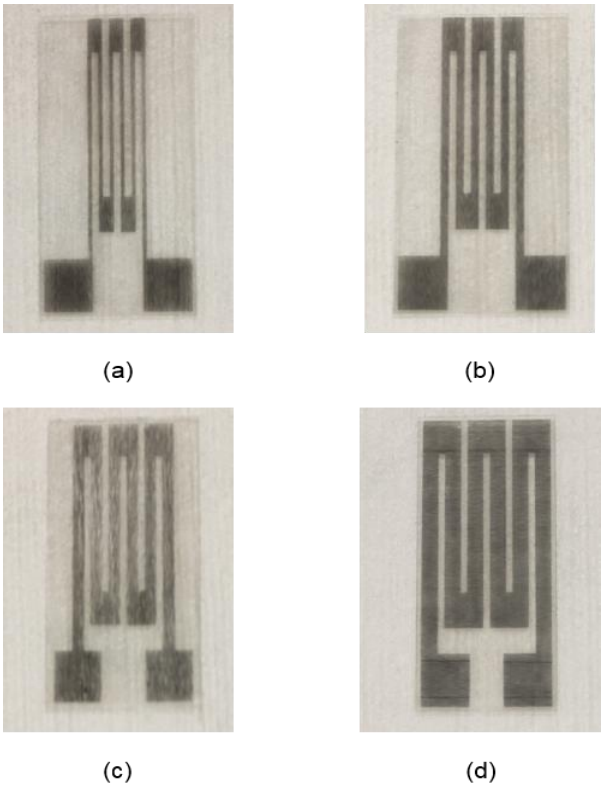

Figure 45. Six grids patterns with different grid width. (a)0.5mm; (b)1mm; (c)1.5mm; (d)2mm.

All samples in this test were 6 grid pattern cross-ply CNTs/PMMA strain sensors. The highest nominal resistance change increased with the width of active grid (except 1mm) as shown in figure 46. Also, the initial resistance decreases with the width of active grid. Therefore, more CNTs make contribution to resistance change during tensile loading if the active gauge grid becomes wider.

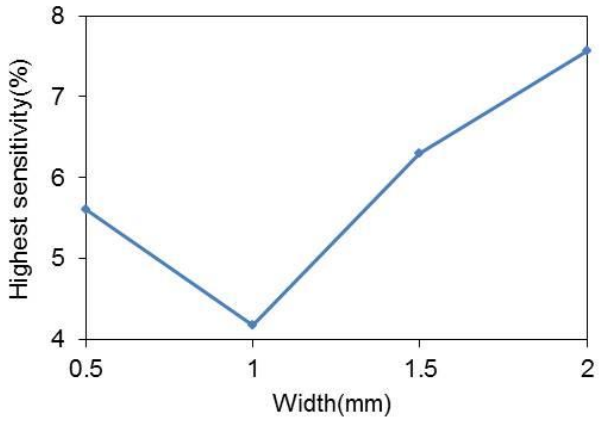

Figure 46. Highest sensitivity of different width comparison.

However, the response of the resistance change for 0.5 mm and 2 mm line widths showed lots noise. Another two tests were carried out on these two samples, but the result still showed the same noise. It is not clear what was creating the noise but it was interesting to see that it was the thinnest and widest grids that showed it.

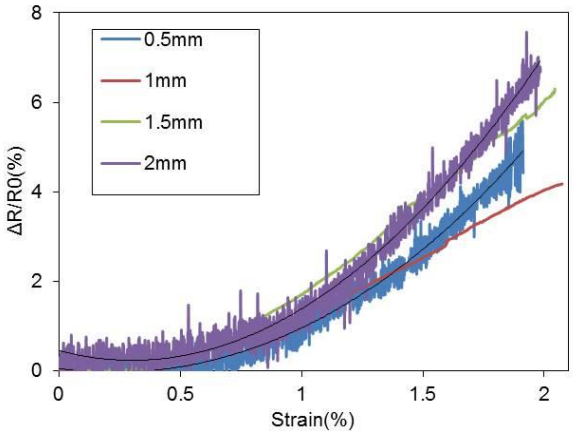

Figure 47. In situ nominal resistance change of different grid width under tensile test.

In order to investigate the effect of the initial resistance on the resistance change, a single layer CNTs/PMMA strain sensor was studied. The single layer CNTs sheet had less electrically conductive pathways and contact points among CNTs than double sheets, thus the initial resistance increased significantly. If the initial resistance was large, it might not be a good material in real application. However, on the other hand, the single CNT sheet samples were less dense than double sheets making them more transparent. Typically the literature shows that higher sensitivity can be obtained from a lower CNTs concentration strain sensor (Rahman & Servati, 2012). However, this may not be the case for our samples because the networked nature of the CNTs in the CNT sheets.

Based on the result shown in figure 48, double layer CNT/PMMA strain sensors showed slightly larger normalized resistance change and also the curve was smoother, whereas, single layer CNT/PMMA strain sensor showed lots of noise.

Table 4. Initial resistance with different number of CNT layer.

Number of layer	1	2
Initial Resistance (kΩ)	62	28

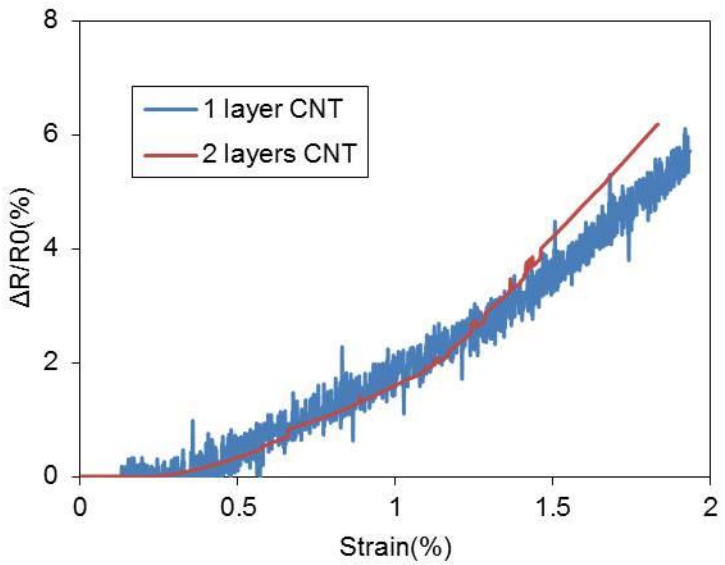

Figure 48. Strain sensitivity comparison between single layer and double layer CNT/PMMA sensors.

The orientation of CNTs within polymer substrates plays an important role in strain sensing capability. In order to study if CNT orientation impacts patterned CNT strain sensor sensitivity, tests on the orientation of CNTs perpendicular and parallel to tensile loading direction were carried out in this study. Double layer CNT/PMMA thin film with 6 grids was used in this test. CNT orientation test results are shown in figure 49.

Table 5. Initial resistance with different orientation of CNTs.

Orientation of CNTs	parallel	perpendicular
Initial Resistance (kΩ)	291	27.95

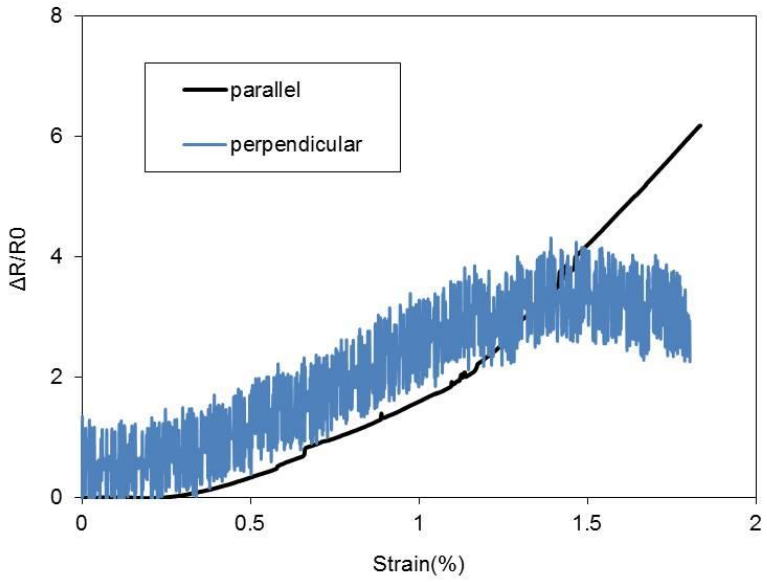

Figure 49. Nominal resistance change of different CNT orientation under tensile test.

Compared to the strain sensors made from CNTs dispersed into polymer solution, our dry-processing aligned CNT sheet/polymer strain sensors showed unique electromechanical strain sensing property. Based on tensile test results, it elucidated that the resistance change of CNT/PMMA strain sensors increases during tensile loading. There are several reasons for the resistance change. In the aligned CNT sheet, nanotubes are densely bundled together to form an electrical network, and thus showing relatively high electrical conductivity. There would be a large number of direct contacts or connections between CNTs. In this particular CNT structure, the resistance between CNTs contact points is much lower than that caused by the tunneling effect of CNTs in close proximity. The relationship between contact resistance and tunneling resistance can be likened to the parallel electrical circuit shown in

figure 50. In this circuit, it contains low resistance (the resistance of CNTs contact area) and high resistance (the resistance caused by tunneling effect) resistors, so the overall circuit resistance is almost dominated by the low resistance element. Thus, the resistance change is more likely dominated by the change of contact points.

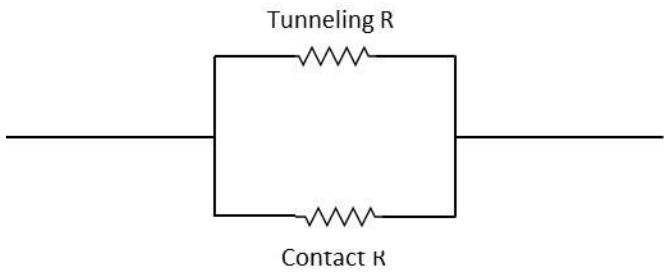

Figure 50. Schematic picture of the relationship between the tunneling resistance and contact resistance among CNTs.

But the overall resistance change is not only attributed to the change of contact points. The geometric change of CNT/polymer strain sensors during tensile loading also has influence on the resistance change. The theory is similar to conventional metal-foil strain gauge. The resistance of the network would increase under tensile strain because of the increase of the length as well as the decrease of the cross-sectional area. On the other hand, during tensile loading, CNTs in the CNT sheet come in closer to each other due to the transverse compressive strain. Thus, the Poisson contraction might be attributed to a decrease in resistance (Li, Bogdanovich, & Bradford, 2015).

However, in the last tensile test, the strain sensors with CNTs parallel and perpendicular to the loading direction did not show much different in terms of strain sensitivity. Therefore, it is thought that the primary reason for resistance change of the strain sensor was the geometric change.

Based on some previous studies in the literature, CNTs embedded into different polymer substrates behavior different in terms of sensitivity. So another substrate polymer PETG was studied to investigate if different substrates have influence on strain sensitivity of the patterned CNT/polymer strain sensor. When identical sensors were produced, the CNT/PETG strain sensor showed much higher normalized resistance change, and also the trend was smoother and more stable as shown in figure 51.

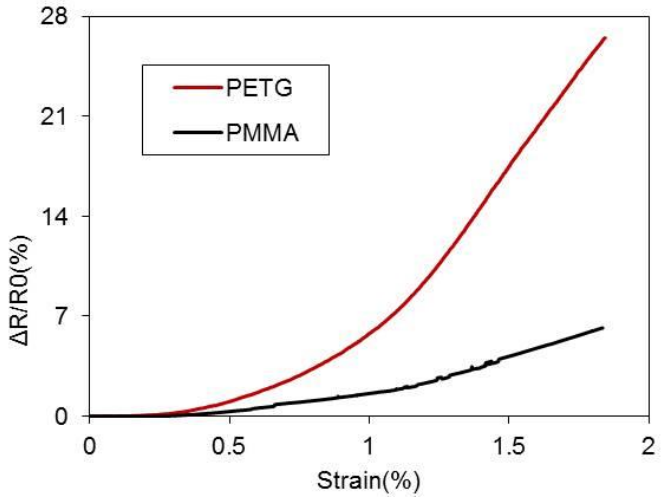

Figure 51. Strain sensitivity of different polymer substrates.

The CNT/PETG strain sensor exhibited much higher sensitivity might be because the methods we chose to embed CNTs into PETG and PMMA were different. PETG might have exhibited better interaction with CNTs, so that CNTs intrinsic piezoresistivity changed during tensile loading. Therefore, the overall resistance change was not only because strain sensor geometric change but also CNT intrinsic piezoresistivity change. It is proven that different polymer substrates dramatically impact the sensitivity.

Another interesting study was conducted to understand the stability of this strain sensor for a long-term usage under a zero mechanical loading condition. A six grid cross-ply CNT/PMMA sensor was mounted on a glass-fiber prepreg composite coupon. Before the long-term test, an initial stabilization test was carried out last for an hour before long-term resistance recording. In total, 29371 data points were collected for 96 hours under room temperature and ambient atmosphere. The final long-term resistance measurement result is shown in figure 52.

The resistance didn’t show large fluctuation during 96 hours measurement, which means this type strain sensor could be used in long-term application. If the resistance changes over time, the literature shows that it is usually an increase due to damage of CNT contact points due to resistive heating. Interestingly, the small resistance change that did occur for the CNT/PMMA sensors decreased the overall resistance.

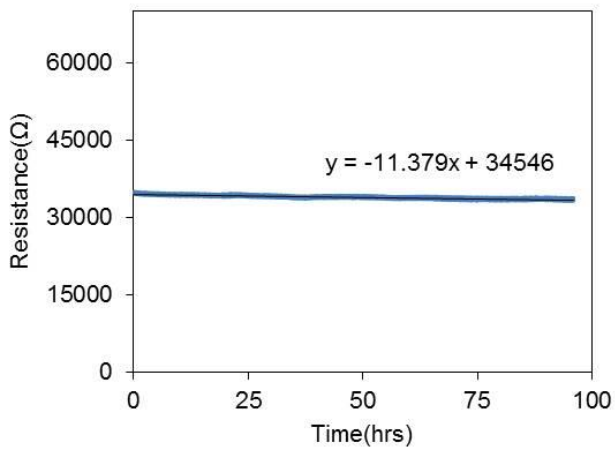

Figure 52. Long-term resistance measurement.

4.3 Other Applications of Etched CNT/polymer Thin Films

Since the CNT/PMMA thin film fabricated in this study is semi-transparent, there is potential for use of these materials in other applications. An experiment was conducted to investigate the resistance behavior of patterned CNT/PMMA thin film under skin touch. A thirty grid pattern with 0.635mm grid width double layers CNT/PMMA thin film was chosen to maximize the electrical resistance change. Figure 53 shows the resistance behavior of this patterned film when a finger was used to contact the sensor. The inset picture shows how the finger contacted the film. The resistance decreased significantly when the finger touched the patterned sensor. The resistance went back to original resistance after released the finger-touched pressure immediately which indicated the resistance was reversible. The contact between the skin and the sensor lines effectively made a short circuit where electrons were allowed to flow either through the grid or across the surface of the skin. This test was stable

and repeatable. Since the CNT/polymer thin film we fabricated was semi-transparent, and showed high sensitivity under pressure, this type of sensor may be able to be employed in touch driven applications.

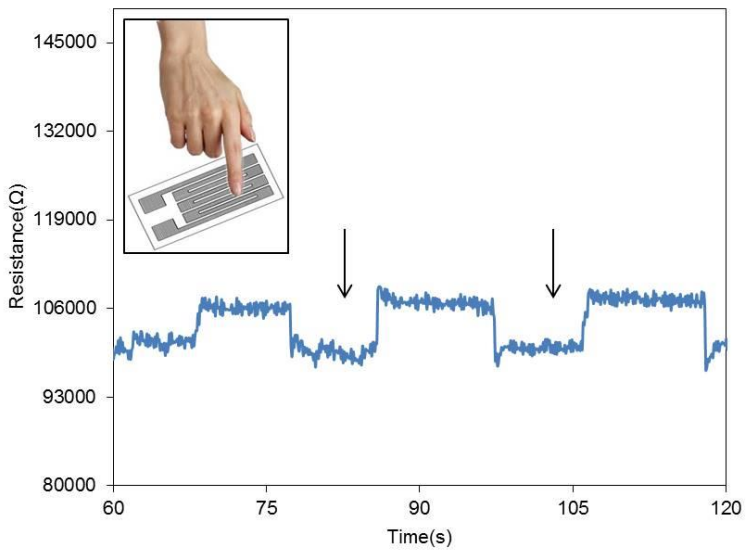

Figure 53. The resistance change of finger touch with pressure.

The temperature sensing function of the thin films was also explored. CNT/PMMA thin film was cut into 1” ×2” with two pieces of 1”×0.5” metal foil attached to the two ends using silver epoxy. Wires were attached to each metal foil using solder. The sample was placed in Isotemp Premium Ovens 700 Series with controlled temperature from 45°C to 100°C. The air-forced oven provided uniform temperature. The operating temperature of this oven could be as high as 275°C. However, the temperature should not go beyond 105°C because the

glass transition temperature of PMMA should not be exceeded. As shown in figure 54, the resistance decreased along with increasing temperature linearly. It suggested that semi-transparent CNT/polymer thin film could also function as a temperature sensor.

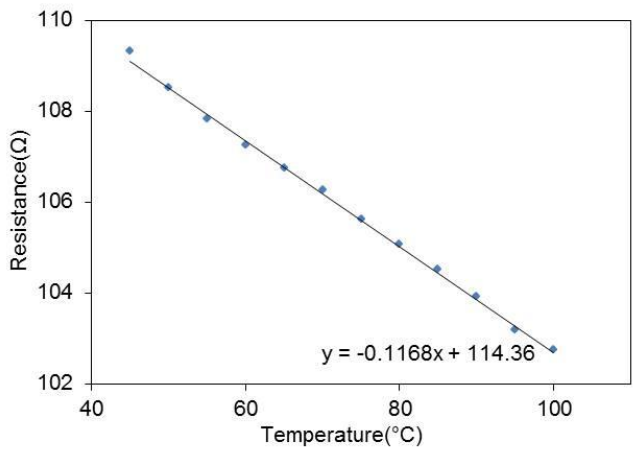

Figure 54. Linear resistance change with increasing temperature.

5 Conclusion

Aligned CNT sheet were embedded into PMMA thin films by heat pressing at 135℃ and 2 tons of force; while embedded into PETG thin films by a calendar roller. The dry-process for fabricating CNT/polymer thin film introduced here was simpler than conventional solution-based process introduced in literature. The CNT surface was etched into a serpentine pattern in a CO_2 laser cutter after CNTs were embedded in the polymer film. The optimal etching power and speed for this set of experiments was 5% etching power (2 watts) and 50% etching speed (40 inches per minute), the CNTs were almost completely etched away while the

polymer surface was only slightly roughened. The transmittance of the etched area reached 87% at 550nm wavelength. The CNT/PMMA thin film was etched into different number of grids and different grid widths. The results showed that the magnitude of resistance change increased but nominal resistance change decreased with the number of grids. The nominal resistance change increased with the width of grid. The tensile test results on different polymer substrates, PETG and PMMA, proved that the polymer substrate impacts sensitivity dramatically. For the CNT/PMMA sensors, the primary reason for the resistance change was strain sensor geometric change; while for CNT/PETG strain sensor, the resistance change was attributed to both geometric change and CNT intrinsic piezoresistivity change. Long-term resistance measurements were conducted for 96 hours and the sensor showed excellent zero-load resistance stability. Some other potential applications such as temperature sensors and pressure sensors were also briefly demonstrated.

6 Future Research

- More effort should be put on decreasing the resistance in the sensor end loops. The resistance of this part should be made as small as possible so that it does not influence the overall starting resistance.
- Sensors should be made that have lower overall resistance. The overall resistance of conventional metal-foil strain gauges is 120Ω or 350Ω. However, for patterned CNT/PMMA strain sensor in this study, the minimum resistance is can be many kΩ. More CNT sheets could be tried to embed into polymer substrate.

- Different polymer substrates could be tried to figure out which one is the most effective at transferring load to the CNTs. From the experiment part, it is proven that CNT embedded into PETG shows higher sensitivity. This shows that polymer plays an important role in sensitivity. More elastic polymers such as PDMS and PU could be tried in following study.
- More flexible and transparent polymers could be investigated as substrates for etched sensors since there is demand for flexible strain sensors.
- More studies should be focusing on different applications of patterned CNT/polymer thin films. The process for fabricating CNT/polymer thin films and laser etching is novel, simple and easy. It could be used in different areas in future.
- Tensile stress might not cause large deformation in CNTs since there very little bonding between CNTs and polymer substrates. The gauge factors we got so far were not as high as we expected. Methods for increasing the interfacial shear strength between CNTs and polymer should be integrated into the fabrication process.

REFERENCES

Arash, B., Wang, Q., & Varadan, V. K. (2014). Mechanical properties of carbon nanotube/polymer composites. *Nature*, 1–8. doi:10.1038/srep06479

Bandaru, P. R. (2007). Electrical properties and applications of carbon nanotube structures. *Journal of Nanoscience and Nanotechnology*, *7*(4-5), 1239–1267. doi:10.1166/jnn.2007.307

Barbour, S. (2014). Surface Modification of Polyester Films with Electrically Conductive Carbon Nanotube Sheets. Retrieved from http://repository.lib.ncsu.edu/ir/handle/1840.16/9883

Beyou, E., Akbar, S., Chaumont, P., & Cassagnau, P. (2013). Polymer nanocomposites containing functionalised multiwalled carbon nanoTubes: a particular attention to polyolefin based materials. *Syntheses and Applications of Carbon Nanotubes and Their Composites*, 77–115. doi:http://dx.doi.org/10.5772/50710

Burdick, Jason A., and Robert L. Mauck. *Biomaterials for Tissue Engineering Applications*. New York, NY: Springer-Verlag/Wien, 2011.

Cai, L., Song, L., Luan, P., Zhang, Q., Zhang, N., Gao, Q., & Zhao, D. (2013). Super-stretchable , Transparent Carbon, 1–9. doi:10.1038/srep03048

Cao, J., Wang, Q., & Dai, H. (2003). Electromechanical properties of metallic, quasimetallic, and semiconducting carbon nanotubes under stretching. *Physical Review Letters*, *90*(15), 157601. doi:10.1103/PhysRevLett.90.157601

Cefic. (2013). Applications and Benefits of Multi-Walled Carbon Nanotubes (MWCNT) Potential Applications, 1–6.

Chang, N.-K., Su, C.-C., & Chang, S.-H. (2008). Fabrication of single-walled carbon nanotube flexible strain sensors with high sensitivity. *Applied Physics Letters*, *92*(6), 063501. doi:10.1063/1.2841669

Chang, W., Song, S., Kim, J., & Kim, J. (n.d.). Transparent film sensor for strain measurement using carbon nanotube networks. *Nsti.org*. Retrieved from http://www.nsti.org/publications/Nanotech/2009/pdf/434.pdf

Che, J., Çagin, T., & Goddard, W. a. (2000). Thermal conductivity of carbon nanotubes. *Nanotechnology*, *11*, 65–69. doi:10.1088/0957-4484/11/2/305

Choudhary, V., & Gupta, A. (2001). Polymer / Carbon Nanotube Nanocomposites. doi:10.5772/18423

Choudhary, V., Singh, B. P., & Mathur, R. B. (2013). Carbon Nanotubes and Their Composites.

Choy, K. (2003). Chemical vapour deposition of coatings. *Progress in Materials Science*, *48*(2), 57–170. doi:10.1016/S0079-6425(01)00009-3

Cueto, E., Ma, a. W. K., Chinesta, F., & Mackley, M. R. (2008). Numerical simulation of spin coating processes involving functionalised Carbon nanotube suspensions. *International Journal of Material Forming*, *1*, 89–99. doi:10.1007/s12289-008-0377-5

Eatemadi, A., Daraee, H., Karimkhanloo, H., Kouhi, M., Zarghami, N., Akbarzadeh, A., … Joo, S. (2014). Carbon nanotubes: properties, synthesis, purification, and medical applications. *Nanoscale Research Letters*, *9*(1), 393. doi:10.1186/1556-276X-9-393

Elastomers, C., Roh, E., Hwang, B., Kim, D., Kim, B., & Lee, N. (2015). Sensor for Human À Machine Interfaces Comprising a Nanohybrid of Carbon, (Xx).

Gau, C., Kuo, C.-Y., & Ko, H. S. (2009). Electron tunneling in carbon nanotube composites. *Nanotechnology*, *20*, 395705. doi:10.1088/0957-4484/20/39/395705

Han, Z., & Fina, A. (2011). Thermal Conductivity of Carbon Nanotubes and Their Polymer Nanocomposites: A Review. *Prog. Polym. Sci.*, *36*(7), 914–944. doi:10.1016/j.progpolymsci.2010.11.004

Hasegawa, S., Shiraki, I., Tanikawa, T., Petersen, C. L., Hansen, T. M., Boggild, P., & Grey, F. (2002). Direct measurement of surface-state conductance by microscopic four-point probe method. *Journal of Physics: Condensed Matter*, *14*(35), 8379–8392. doi:10.1088/0953-8984/14/35/309

Heyd, R., Charlier, a., & McRae, E. (1997). Uniaxial-stress effects on the electronic properties of carbon nanotubes. *Phys. Rev. B*, *55*(11), 6820–6824. doi:10.1103/PhysRevB.55.6820

Hu, N., Masuda, Z., Yan, C., Yamamoto, G., Fukunaga, H., & Hashida, T. (2008). The electrical properties of polymer nanocomposites with carbon nanotube fillers. *Nanotechnology*, *19*, 215701. doi:10.1088/0957-4484/19/21/215701

Huang, Y. T., Huang, S. C., Hsu, C. C., Chao, R. M., & Vu, T. K. (2012). Design and fabrication of single-walled carbon nanonet flexible strain sensors. *Sensors*, *12*, 3269–3280. doi:10.3390/s120303269

Huynh, C. P., & Hawkins, S. C. (2010). Understanding the synthesis of directly spinnable carbon nanotube forests. *Carbon*, *48*(4), 1105–1115. doi:10.1016/j.carbon.2009.11.032

Jiang, K., Wang, J., Li, Q., Liu, L., Liu, C., & Fan, S. (2011). Superaligned carbon nanotube arrays, films, and yarns: A road to applications. *Advanced Materials*, *23*, 1154–1161. doi:10.1002/adma.201003989

Jin, L., Bower, C., & Zhou, O. (1998). Alignment of carbon nanotubes in a polymer matrix by mechanical stretching. *Applied Physics Letters*, *73*(1998), 1197–1199. doi:10.1063/1.122125

Jones, R. M. (1999). Mechanics of Composite Materials. *Mechanics of Composite Materials*, *18*(4), 519. doi:10.1007/BF00611782

Joo, M., & Lee, M. (2012). High-quality parallel patterning of carbon nanotube thin films by a pulsed laser beam. *Thin Solid Films*, *520*(11), 3971–3974. doi:10.1016/j.tsf.2012.01.025

Jung, D., Lee, K. H., Overzetand, L. J., & Lee, G. S. (2012). A High Sensitive Strain Sensor using a Multi-walled Carbon Nanotube Sheet Experimental set-up Characterization Synthesis of the MWCNT sheet.

Kang, I., Schulz, M. J., Kim, J. H., Shanov, V., & Shi, D. (2006). A carbon nanotube strain sensor for structural health monitoring. *Smart Materials and Structures*, *15*(3), 737–748. doi:10.1088/0964-1726/15/3/009

Kanoun, O., Müller, C., Benchirouf, A., Sanli, A., Dinh, T., Al-Hamry, A., … Bouhamed, A. (2014a). Flexible Carbon Nanotube Films for High Performance Strain Sensors. *Sensors*, *14*, 10042–10071. doi:10.3390/s140610042

Kanoun, O., Müller, C., Benchirouf, A., Sanli, A., Dinh, T. N., Al-Hamry, A., … Bouhamed, A. (2014b). Flexible carbon nanotube films for high performance strain sensors. *Sensors (Basel, Switzerland)*, *14*(6), 10042–71. doi:10.3390/s140610042

Khan, A. S., & Wang, X. (2001). Strain measurements and stress analysis. Retrieved from http://www.bcin.ca/Interface/openbcin.cgi?submit=submit&Chinkey=210249

Kim, D., & Yun, K. S. (2013). Patterning of carbon nanotube films on PDMS using SU-8 microstructures. *Microsystem Technologies*, *19*(5), 743–748. doi:10.1007/s00542-012-1677-8

Kumar, M., & Ando, Y. (2010). Chemical vapor deposition of carbon nanotubes: a review on growth mechanism and mass production. *Journal of Nanoscience and Nanotechnology*, *10*(6), 3739–3758. doi:10.1166/jnn.2010.2939

Kuznetsov, A. a., Fonseca, A. F., Baughman, R. H., & Zakhidov, A. a. (2011). Structural model for dry-drawing of sheets and yarns from carbon nanotube forests. *ACS Nano*, *5*(2), 985–993. doi:10.1021/nn102405u

Lee, D., Hong, H. P., Lee, C. J., Park, C. W., & Min, N. K. (2011). Microfabrication and characterization of spray-coated single-wall carbon nanotube film strain gauges. *Nanotechnology*, *22*, 455301. doi:10.1088/0957-4484/22/45/455301

Lepró, X., Lima, M. D., & Baughman, R. H. (2010). Spinnable carbon nanotube forests grown on thin, flexible metallic substrates. *Carbon*, *48*(12), 3621–3627. doi:10.1016/j.carbon.2010.06.016

Li, A., Bogdanovich, A. E., & Bradford, P. D. (1866). Aligned Carbon Nanotube Sheet Piezoresistive Strain Sensors, 1–29.

Lin, H. K., Lin, R. C., & Li, C. H. (2010). Etching processes of transparent carbon nanotube thin films using laser technologies. *Thin Solid Films*, *518*(24), 7253–7257. doi:10.1016/j.tsf.2010.04.094

M.N.Avadhanulu. (2007). *S.Chand Engineering Physics*. S. Chand Limited. Retrieved from https://books.google.com/books?id=hjeGvMLlWFsC&pgis=1

Majumder, M. K., Kaushik, B. K., & Manhas, S. K. (2011). Performance comparison between single wall carbon nanotube bundle and multiwall carbon nanotube for global interconnects. *2011 International Conference on Emerging Trends in Networks and Computer Communications (ETNCC)*, 104–109. doi:10.1109/ETNCC.2011.5958496

Minot, E. D., Yaish, Y., Sazonova, V., Park, J.-Y., Brink, M., & McEuen, P. L. (2003). Tuning carbon nanotube band gaps with strain. *Physical Review Letters*, *90*(15), 156401. doi:10.1103/PhysRevLett.90.156401

Mirri, F., Ma, A. W. K., Hsu, T. T., Behabtu, N., Eichmann, S. L., Young, C. C., … Pasquali, M. (2012). High-performance carbon nanotube transparent conductive films by scalable dip coating. *ACS Nano*, *6*(11), 9737–9744. doi:10.1021/nn303201g

Moniruzzaman, M., & Winey, K. I. (2006). Polymer Nanocomposites Containing Carbon Nanotubes. *Macromolecules*, *39*(16), 5194–5205. doi:10.1021/ma060733p

Moshkalyov, S. a., Moreau, a. L. D., Guttiérrez, H. R., Cotta, M. a., & Swart, J. W. (2004). Carbon nanotubes growth by chemical vapor deposition using thin film nickel catalyst. *Materials Science and Engineering: B*, *112*, 147–153. doi:10.1016/j.mseb.2004.05.038

Nessim, G. D. (2010). Properties, synthesis, and growth mechanisms of carbon nanotubes with special focus on thermal chemical vapor deposition. *Nanoscale*, *2*, 1306–1323. doi:10.1039/b9nr00427k

O'Connell, M. J. (2006). *Carbon Nanotubes: Properties and Applications*. CRC Press. Retrieved from https://books.google.com/books?id=xdhh0ryJRc8C&pgis=1

Obitayo, W., & Liu, T. (2012). A review: Carbon nanotube-based piezoresistive strain sensors. *Journal of Sensors*, *2012*. doi:10.1155/2012/652438

Oliva-Avilés, a. I., Avilés, F., & Sosa, V. (2011). Electrical and piezoresistive properties of multi-walled carbon nanotube/polymer composite films aligned by an electric field. *Carbon*, *49*, 2989–2997. doi:10.1016/j.carbon.2011.03.017

Pang, C., Lee, G.-Y., Kim, T., Kim, S. M., Kim, H. N., Ahn, S.-H., & Suh, K.-Y. (2012). A flexible and highly sensitive strain-gauge sensor using reversible interlocking of nanofibres. *Nature Materials*, *11*(September), 795–801. doi:10.1038/nmat3380

Prasek, J., Drbohlavova, J., Chomoucka, J., Hubalek, J., Jasek, O., Adam, V., & Kizek, R. (2011). Methods for carbon nanotubes synthesis—review. *Journal of Materials Chemistry*, *21*, 15872. doi:10.1039/c1jm12254a

Rafique, M. M. A., & Iqbal, J. (2011a). Production of Carbon Nanotubes by Different Routes — A Review. *Journal of Encapsulation and Adsorption Science*, *1*(June), 29–34. doi:10.4236/jeas.2011.11004

Rafique, M. M. A., & Iqbal, J. (2011b). Production of Carbon Nanotubes by Different Routes-A Review. *Journal of Encapsulation and Adsorption Sciences*, *01*(02), 29–34. doi:10.4236/jeas.2011.12004

Rahman, R., & Servati, P. (2012). Effects of inter-tube distance and alignment on tunnelling resistance and strain sensitivity of nanotube/polymer composite films. *Nanotechnology*, *23*(5), 055703. doi:10.1088/0957-4484/23/5/055703

Rao, C. N. R., Voggu, R., & Govindaraj, a. (2009). Selective generation of single-walled carbon nanotubes with metallic, semiconducting and other unique electronic properties. *Nanoscale*, *1*, 96–105. doi:10.1039/b9nr00104b

Saha, A., Jiang, C., & Martí, A. a. (2014). Carbon nanotube networks on different platforms. *Carbon*, *79*, 1–18. doi:10.1016/j.carbon.2014.07.060

Saotome, T., Kim, H., Wang, Z., Lashmore, D., & Hahn, H. T. (2011). Transparent conducting film: Effect of vacuum filtration of carbon nanotube suspended in oleum. *Bulletin of Materials Science*, *34*(4), 623–628. doi:10.1007/s12034-011-0172-7

Sarkar, A., & Hah, D. (2012). Electrophoretic deposition of carbon nanotubes on silicon substrates. *Journal of Electronic Materials*, *41*(11), 3130–3138. doi:10.1007/s11664-012-2237-9

Schulz, Mark, Vesselin Shanov, and Zhangzhang Yin. *Nanotube Superfiber Materials: Changing Engineering Design*. William Andrew, 2013. Web.

Slobodian, P. (2012). A highly-deformable composite composed of an entangled network of electrically-conductive carbon-nanotubes embedded in elastic polyurethane. *Carbon*, *50*(10), 3446–3453. doi:10.1016/j.carbon.2012.03.008

Thomas, S., & Zaikov, G. E. (2008a). *Polymer Nanocomposite Research Advances*. Nova Publishers. Retrieved from https://books.google.com/books?id=FU5Gtb5EBZ0C&pgis=1

Thomas, S., & Zaikov, G. E. (2008b). *Polymer Nanocomposite Research Advances*. Nova Publishers. Retrieved from https://books.google.com/books?hl=en&lr=&id=FU5Gtb5EBZ0C&pgis=1

Times, S., & Central, P. (2009). Advancements in spinnable CNT arrays.

Vemuru, S. M., Wahi, R., Nagarajaiah, S., & Ajayan, P. M. (2009). Strain sensing using a multiwalled carbon nanotube film. *The Journal of Strain Analysis for Engineering Design*, *44*(7), 555–562. doi:10.1243/03093247JSA535

Xu, W., & Allen, M. G. (2013). Deformable strain sensors based on patterned MWCNTs/polydimethylsiloxane composites. *Journal of Polymer Science, Part B: Polymer Physics*, *51*, 1505–1512. doi:10.1002/polb.23361

Yamada, T., Hayamizu, Y., Yamamoto, Y., Yomogida, Y., Izadi-Najafabadi, A., Futaba, D. N., & Hata, K. (2011). A streYamada, T., Hayamizu, Y., Yamamoto, Y., Yomogida, Y.,

Izadi-Najafabadi, A., Futaba, D. N., & Hata, K. (2011). A stretchable carbon nanotube strain sensor for human-motion detection. Nature Nanotechnology, 6(5), 296–301. doi:10.1038/nnano.2011.36tcha. *Nature Nanotechnology*, *6*(5), 296–301. doi:10.1038/nnano.2011.36

Yildiz, O., & Bradford, P. D. (2013). Aligned carbon nanotube sheet high efficiency particulate air filters. *Carbon*, *64*, 295–304. doi:10.1016/j.carbon.2013.07.066

Yong, L. I., Wanlu, W., Kejun, L., & Chenguo, H. U. (2003). Piezoresistive effect in carbon nanotube films. *Chinese Science Bulletin*, *48*(2), 11–13. doi:10.1021/nn503596f

APPENDICES

Appendix A

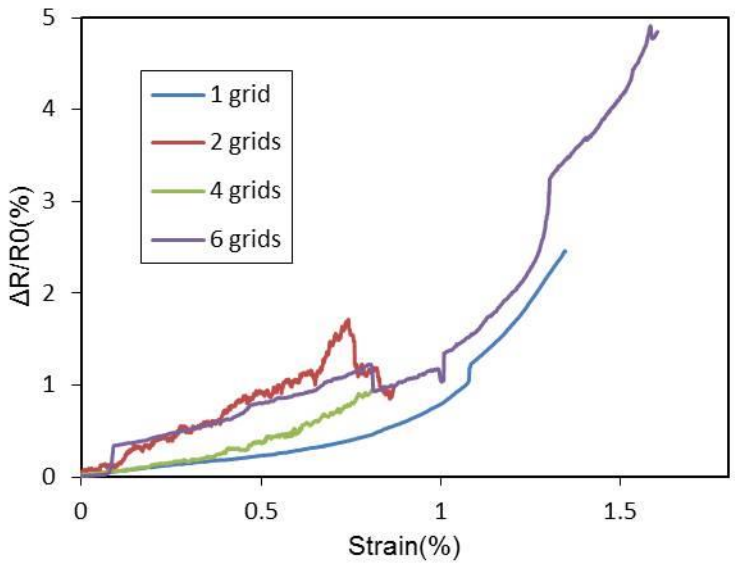

Figure 55. In situ nominal resistance change of different number of grids on acrylic coupon under tensile test.